A macrocyclic peptide-based fusion inhibitor targeting SARS-CoV-2 Spike S2 subunit

Hirofumi Ohashi[1#], Tatsuro Kawamura[2#], Masaki Ohuchi[2], Haruaki Kurasaki[2], Naoko Iwata-Yoshikawa[3], Yuichiro Hirata[3], Saya Moriyama[4], Kaho Shionoya[1], Kazutaka Nagatomo[2], Takayuki Nagasawa[2], Junpei Yamamoto[2], Kei Sudo[2], Naoko Nakamura[2], Katsuma Matsui[2], Haruhiko Ogawa[2], Kouji Yoshida[2], Yoshiaki Shimada[2], Tomoko Maruyama[2], Tomoaki Higuchi[2], Shoko Ito[2], Yoshimasa Takahashi[4], Naoki Kawamura[2], Patrick C. Reid[2], Masato Murakami[2,5], Tadaki Suzuki[3,6], Noriyo Nagata[3]*, Hidetomo Kitamura[2]*, Koichi Watashi[1]*

[1]Department of Drug Development, National Institute of Infectious Diseases, Japan Institute for Health Security, Japan

[2]PeptiDream Inc., Japan

[3]Department of Infectious Disease Pathology, National Institute of Infectious Diseases, Japan Institute for Health Security, Japan

[4]Research Center for Vaccine Development, National Institute of Infectious Diseases, Japan Institute for Health Security, Japan

[5]PeptiAid Inc., Japan

[6]Department of Infectious Disease Pathobiology, Graduate School of Medicine, Chiba University, Japan

[#]These authors contributed equally: Hirofumi Ohashi, Tatsuro Kawamura.

*Corresponding authors:

E-mail: nagata.no@jihs.go.jp (N.Nagata), hidetomo-kitamura@peptidream.com (H.Kitamura), watashi.k@jihs.go.jp (K.W.)

Abstract

Continuous emergence of SARS-CoV-2 variants carrying mutations in Spike presents a significant challenge for durable antiviral agents. Here we screen for random 13-amino acid non-mimetic macrocyclic peptides that bind to Spike and identify PA-001 that inhibits SARS-CoV-2 infection with high potency at 0.23–2.9 nM as 50% inhibitory concentration (IC_{50}). PA-001 bound to Spike S2 subunit and inhibited the membrane fusion during virus entry. Through drug-resistant selection, we revealed that PA-001 targeted the fusion peptide proximal region (FPPR) in S2, which has not been recognized as a drug target to date. Consistent with its highly conserved amino acid sequences beyond strains, PA-001 exhibited broad antiviral activity against all tested SARS-CoV-2 variants, in contrast to clinically-approved S1-targeting antibodies that lost activity to Omicron variants. PA-001 suppressed SARS-CoV-2 propagation and disease progression in mouse- and hamster-infection models, both by administration prophylactically and therapeutically. Combination therapy with remdesivir further enhanced antiviral profiles. In clinical phase-I trial, PA-001 was well-tolerated and showed high systemic exposure, with 4,300–10,300-fold concentration of IC_{50} as maximum plasma concentration by single administration to healthy volunteers. These evidence propose FPPR as an unexpected antiviral drug target accessible by macrocyclic peptides and identify PA-001 as a potent anti-SARS-CoV-2 fusion inhibitor.

Introduction

Coronavirus disease 2019 (COVID-19), caused by infection with severe acute respiratory syndrome coronavirus 2 (SARS-CoV-2), has had a profound impact on global public health, resulting in more than 770 million cumulative cases and over 7 million deaths worldwide (https://covid19.who.int/). Despite the development and widespread deployment of vaccines and antiviral drugs, COVID-19 continues to impose a substantial disease burden, especially among people including older adults, individuals with underlying medical conditions, and immunocompromised populations[1-3]. Throughout and beyond the pandemic period, SARS-CoV-2 has exhibited continuous viral evolution, given rise to numerous variants characterized by the accumulated mutations[4]. These genetic changes have altered viral pathogenicity and transmissibility and, critically, reduced susceptibility to approved antiviral drugs. There is a need to develop novel antiviral agents sustainably retaining their efficacy against ongoing emergence of SARS-CoV-2 variants.

The Spike glycoprotein of SARS-CoV-2 mediates viral entry to host cells through receptor binding and membrane fusion. Spike constitutes a trimeric precursor and comprises two functional subunits, S1 and S2. S1 consists of N-terminal domain (NTD), receptor binding domain (RBD), and C-terminal domains (CTDs), and is essential for recognition of host entry receptor, angiotensin converting enzyme 2 (ACE2), through its RBD[5,6]. S2 contains multiple functional domains including fusion peptide (FP) and its proximal region (FPPR), heptad repeat 1 (HR1), central helix (CH), connector domain (CD), heptad repeat 2 (HR2), and transmembrane domain (TMD) (see Fig. 2E)[4,6]. Upon RBD in the S1 subunit engagement to ACE2, S2 is processed at its N-terminal S2′ site by host proteases, either transmembrane serine protease 2 (TMPRSS2) on the cell surface or cathepsin L in the endosome, which then induces large-scale conformational rearrangements of S2 in the membrane fusion process (Supplementary Fig. 1)[6-12]: The S1-ACE2 complex dissociates from the S2 trimer (Supplementary Fig. 1a-c), and the original conformation (pre-fusion form) of S2 is converted to forms a long central coiled coil with blunted cone-shaped structure (involving FP and the adjacent FPPR) at its top, which allows insertion into the target cell membrane (Intermediation form; Supplementary Fig. 1d). It subsequently refolds into the stable structure by interaction of HR1 and HR2 to form a six-helix bundle that constitutes a rigid, rod-like shape (Post-fusion form; Supplementary Fig. 1e-f) to undergo fusion of viral envelope to cellular membranes.

This viral entry process is an attractive antiviral target[13]. The clinically-approved antibodies for COVID-19 treatment, such as casirivimab, imdevimab, sotrovimab, tixagevimab, cilgavimab, and bebtelovimab, recognize the S1 subunit and are designed to strongly block the S1 RBD-ACE2 binding[14,15]. However, their neutralization activities have been lost by accumulated mutations, especially in RBD, in the recent Omicron subvariants such as BQ.1 and XBB[16]. Other S1-targeting antibodies, including those targeting NTD, also face the similar challenges for emerging escape variants due to high sequence variability in this region. Given its highly conserved

86 sequence among circulating SARS-CoV-2 variants, S2 is expected as an alternative target for
87 broadly active antivirals. So far, S2-targeting antibodies have been identified, including those
88 recognizing the region downstream of the S2′ cleavage site (used to be referred as FP, but is
89 presently defined an intermediate loop) and the stem helix at the upstream of HR2[17-19], but their
90 neutralizing activities were typically low compared to those targeting RBD in S1. So far, peptides
91 mimicking the HR2 sequence aiming to inhibit HR1-HR2 interaction during the conversion to the
92 post-fusion form have been under clinical development. These peptides have shown broad anti-
93 SARS-CoV-2 activity, but their original activities of pre-optimized peptides were 500-3,000 nM
94 ranges as 50% inhibitory concentrations (IC_{50})[18,20]. Later, these S2-mimicking linear peptides
95 have been optimized for improving their activities through polyethylene glycol or cholesterol
96 conjugations. These antibody- and linear peptide-based approaches face a challenge in which
97 their target site as well as antiviral activities are limited due to the S2's inherent characteristics
98 including limited surface area accessibility by large molecules as well as low immunogenicity and
99 high flexibility.
100 Cyclic peptide-based drugs are expected to provide an alternative approach[21] that can have
101 drug-like properties and advantages including accessibility to narrow target sites, high specificity,
102 tunable stability and efficacy, low immunogenicity, and relatively less cost compared to antibodies.
103 In this study, we show that a non-mimetic macrocyclic peptide, PA-001, inhibits infection of broad
104 SARS-CoV-2 variants via targeting FPPR within the S2 subunit, which is highly conserved in
105 sequence but previously undescribed as a druggable site. By using SARS-CoV-2-inoculated
106 mouse and hamster models, PA-001 suppressed viral propagation and ameliorated disease
107 progression under administrations either prophylactically or therapeutically. A first-in-human
108 Phase I dose-escalation trial demonstrated a favorable safety profile with high systemic exposure
109 in pharmacokinetics (achieving maximum plasma concentration of over 4,000-fold concentration
110 of in vitro IC_{50} against Omicron strains) in healthy volunteers. Our findings present PA-001 as
111 an anti-SARS-CoV-2 drug candidate and that FPPR is a potential druggable target for SARS-CoV-
112 2 fusion inhibitor.
113
114
115 **Results**
116 **Identification of an anti-SARS-CoV-2 cyclic peptide, PA-001**
117 To explore novel COVID-19 therapy targeting SARS-CoV-2 Spike, we discovered and
118 developed anti-SARS-CoV-2 agents following the scheme as summarized in Fig. 1A. Through
119 screening of a library consisting of ~10^{13} random peptides using Peptide Discovery Platform
120 System (PDPS), which we have established so far[22-24] (Fig. 1B), and the following rational
121 optimization process through medicinal-chemistry program, we developed PA-001 (Fig. 1C) as an
122 investigational agent currently in clinical development as a therapy against COVID-19. In the
123 present study, we report the in vitro and in vivo antiviral profile of PA-001.

124 Peptides that were identified to bind Spike in vitro were optimized to improve antiviral potency
125 and pharmacokinetics (Fig. 1A). We examined i) affinity with Spike in vitro (Supplementary Table
126 1), ii) inhibition activity to SARS-CoV-2 infection in a cell-based assay (Fig. 1D), and iii)
127 pharmacokinetics profiles in mice (Fig. 1E). In surface plasmon resonance, PA-001 had high
128 affinity to recombinant Spike, with 1.3 nM as a K_D (Supplementary Table 1). Activity of peptides
129 to inhibit SARS-CoV-2 infection was examined in a cell-based SARS-CoV-2 infection assay:
130 VeroE6/TMPRSS2 cells[25] were inoculated with a SARS-CoV-2 clinical isolate (Wk-5.2.1, Wuhan
131 type) at a multiplicity of infection (MOI) of 0.003 for 1 h and were cultured in the presence or
132 absence of peptides for 48 h to assess SARS-CoV-2-induced cytopathology (Fig. 1D). The cell
133 line exhibited robust cytopathology by SARS-CoV-2 propagation at 48 h after infection, which was
134 however completely blocked by treatment with 50 nM PA-001, as 10 μM remdesivir (RDV), a
135 clinically-approved anti-SARS-CoV-2 polymerase inhibitor[26] used as a positive control (Fig. 1D-
136 b). PA-001 reduced the production of SARS-CoV-2 proteins, Spike and N as representatives
137 detected by immunoblotting, at 24 h post-inoculation, the time before showing cytopathic effect
138 (Fig. 1D-c). PA-001 reduced viral RNA at 24 h post-inoculation in a dose-dependent manner (Fig.
139 1D-d). Pharmacokinetics of a single intraperitoneal administration with PA-001 at 10 mg/kg to
140 BALB/c mice showed 76,667 ng/mL (41,500 nM) as maximum plasma concentration (C_{max}) and a
141 gradual decline but sustained plasma concentration, with 1.0 h as half-life, and 282,236 ng·h/mL
142 (153,000 nM·h) as area under the curve (AUC_{0-24}) in plasma (Fig. 1E, Supplementary Table 2).
143 From these data showing the strong potential of PA-001 as an anti-SARS-CoV-2 agent, we
144 focused on PA-001 in the following analysis.
145
146 **PA-001 targets S2 and inhibits Spike-dependent membrane fusion**
147 We determined the target of PA-001 by in vitro binding assay that incubated PA-001 at varying
148 concentrations with recombinant either full-length (S1+S2), S1, or S2 protein as targets. As
149 shown in Fig. 2A, PA-001 presented the binding signal with the full-length Spike and S2 in a dose-
150 dependent manner, but not with S1 at any treated concentrations up to 100 nM (Fig. 2A),
151 suggesting that PA-001 binds to S2. In the SARS-CoV-2 life cycle, cell entry is initiated by viral
152 attachment to cells through binding of S1 RBD to ACE2 on cell surface (Fig. 2B, red); This is
153 followed by the fusion of viral envelope with cellular membranes either on cell surface or at
154 intracellular vesicles, triggered by cleavage of the S2 internal site (S2′ site) by cellular proteases
155 (Fig. 2B, brown). To confirm the target step of PA-001 during the entry process, we separately
156 assessed the activity of viral attachment to cell surface (Fig. 2C-a) and membrane fusion (Fig.
157 2C-b). Attachment assay was performed by incubating VeroE6/TMPRSS2 cells with SARS-CoV-
158 2 at 4°C to allow viral-cell attachment but not the following processes, followed by quantification
159 of viral RNA on the cell surface. Cell-attached SARS-CoV-2 RNA was dose-dependently
160 reduced upon treatment with casirivimab + imdevimab (CAS + IMD) cocktail antibodies, clinically-
161 approved SARS-CoV-2 neutralizing antibodies[27] used as a positive control, whereas that was not

162 significantly affected by treatment with PA-001, as with mefloquine, a reported post-attachment
163 entry inhibitor[28] used as a negative control (Fig. 2C-a). On the other hand, in the cell fusion
164 assay, which coincubated Spike-overexpressing HEK293T cells with endogenously ACE2-
165 expressing VeroE6/TMPRSS2 cells to induce cell membrane fusion, essentially as previously
166 described[29], PA-001 clearly reduced Spike-ACE2-induced fusion in a dose-dependent manner,
167 and its IC_{50} was calculated to be 3.6 nM (Fig. 2C-b). These results are consistent with that PA-
168 001 targets S2, which mediates the membrane fusion process.
169 To identify the S2 target site responsible for the PA-001 sensitivity, we isolated PA-001-resistant
170 SARS-CoV-2 variants by continuous exposure of SARS-CoV-2-infected cells with PA-001 and
171 serial passages, essentially described previously[30] (Fig. 2D-a): VeroE6/TMPRSS2 cells infected
172 with SARS-CoV-2 were continuously treated with PA-001 and their culture supernatant was
173 reinfected to naive VeroE6/TMPRSS2 cells. After seven passages, we collected SARS-CoV-2
174 in the culture supernatant from eight independent cell batches (A8, B8, C8, D8, E8, F8, G8, and
175 H8). We then examined the sensitivity of these virus clones to PA-001, as well as RDV as a
176 reference, by inoculating the cells with these viruses or the parental wild type SARS-CoV-2 and
177 treated with PA-001 or RDV at varying concentrations to quantify viral RNA produced into the
178 culture supernatant. As shown in Fig. 2D-b, all the virus clones (A8-H8) showed no or limited
179 reduction in viral RNA levels by treatment with PA-001 up to 500 nM, in contrast to the drastic
180 reduction in RNA of the parental SARS-CoV-2 (Fig. 2D-b left, and Supplementary Fig. 2A-a). In
181 contrast, all these variants remained sensitive to RDV, as the parental SARS-CoV-2 (Fig. 2D-b
182 right, Supplementary Fig. 2A-b). The calculated 90% inhibitory concentrations (IC_{90}s) to PA-001
183 for all the clones were >500 nM (v.s. 8.4 nM for the parental virus), whereas those to RDV for all
184 clones remained 3,000-4,500 nM that were equivalent to the parental virus (Supplementary Fig.
185 2B), indicating that all the isolated variants acquired specific resistance to PA-001.
186 Next-generation sequencing of viral RNA derived from these eight clones identified 1-3 amino
187 acid substitutions for each clone, with enriched substitutions in the S2 region (Supplementary Fig.
188 2C), consistent with that PA-001 targets S2. Interestingly, D8 and H8 had the identical and single
189 mutation that caused amino acid substitution, L841R in S2 protein (Fig. 2E-a, Supplementary Fig.
190 2C), suggesting that the L841R substitution is responsible for acquiring the PA-001 resistance.
191 Similarly, E8 and G8 possessed the identical but another single amino acid substitution, P862Q
192 in S2 (Fig. 2E-a, Supplementary Fig. 2C). Remarkably, all the remaining clones also acquired a
193 substitution cluster at the neighboring amino acids, Q836 (in F8), Y837 (in A8 and F8), G838 (in
194 B8), and L858 (in C8) (Fig. 2E-a highlighted by pink, Supplementary Fig. 2C). All these amino
195 acids reside at the upstream of the fusion peptide (FP: 866-910 aa) in S2, referred as the fusion
196 peptide proximal region (FPPR)[4,6-9] (Fig. 2E-a). Based on the reported three-dimensional
197 structure of Spike protein at pre-fusion, intermediation, and post-fusion forms[10-12], FPPR
198 dynamically moves and changes its structure, together with FP, during the conversion from the
199 pre-fusion to the post-fusion form[4]: FPPR is originally exposed on the surface in a concave area

200 of the central part of the pre-fusion trimer, and undergoes a dynamic locational change to the top
201 of S2, forming the cone-shaped structure to assist FP insertion into target membrane in the post-
202 fusion form[11] (Fig. 2E-b).
203 As the above critical amino acids, Q836, Y837, G838, L841, L858, and P862 are exposed on
204 the surface of the Spike pre-fusion trimer, we assume these amino acids constitute the interface
205 to PA-001 binding, of which amino acid substitutions lead to escape from PA-001 binding. We
206 then examined the binding activity of recombinant Spike having a substitution of either L841R (in
207 D8 and H8) or P862Q (in E8 and G8) to PA-001 by ELISA: Spike proteins were immobilized on
208 the well, and incubated with varying amount of HA-tagged PA-001, which was then visualized by
209 adding anti-HA-conjugated horseradish peroxidase (HRP). Specific Spike-PA-001 binding was
210 evaluated by the difference in the signal from that under coincubation with and without excess
211 amount of non-HA-tagged PA-001 as a competitor (Fig. 2F-a). This specific Spike-PA-001
212 binding was observed along with the increasing amount of PA-001-HA by using the wild type Spike,
213 however, this signal completely disappeared for Spike carrying the substitution at either L841R or
214 P862Q (Fig. 2F-b), suggesting that these amino acid substitutions abrogate PA-001 binding.
215 Consistently, PA-001's dose-dependent inhibition of the Spike-ACE2-mediated cell membrane
216 fusion was totally cancelled up to 1,000 nM by mutations of L841R or P862Q in Spike (Fig. 2G).
217 These data cumulatively suggest that PA-001 binds to FPPR to inhibit S2-dependent membrane
218 fusion.
219
220 **PA-001 shows antiviral activity to broad range of SARS-CoV-2 variants**
221 Multiple neutralizing antibodies have been approved for clinical use, however, all of them have
222 lost antiviral efficacy by amino acid substitutions in Spike observed in naturally-occurring SARS-
223 CoV-2 variants[14,31]. Most of these substitutions were concentrated in the S1 subunit. To clarify
224 the breadth of the antiviral activity of PA-001, we infected VeroE6/TMPRSS2 cells with SARS-
225 CoV-2 Wuhan, Alpha, Beta, Gamma, Delta, and Omicron (BA.1.18 and XBB.1.16), and treated
226 with varying concentrations of PA-001 as well as CAS + IMD as a reference to quantify viral RNA
227 in the culture supernatant. As previously reported, CAS + IMD showed antiviral effects on
228 Wuhan to Delta variants, but not Omicron variants (Fig. 3A, lower graphs), because of the amino
229 acid substitutions in RBD of S1[32,33]. In contrast, PA-001 reduced SARS-CoV-2 infection for all
230 the variants examined including Omicron variants, BA.1.18 and XBB.1.16, in a dose-dependent
231 manner (Fig. 3A, upper graphs). Anti-SARS-CoV-2 activities of PA-001 against all these variants
232 ranged 0.23-2.9 nM as IC_{50}s and 1.3-9.4 nM as IC_{90}s, in contrast to the complete loss of activity
233 of CAS + IMD against BA.1.18 and XBB.1.16 (IC_{50} and IC_{90} >1,000 ng/mL) (Supplementary Table
234 3). Furthermore, PA-001 showed the inhibitory activity to the recent Omicron subvariants, JN.1
235 and XFG, in contrast to loss of activity of CAS + IMD, examined by infection of VSV-based
236 pseudovirus carrying Spike derived from each SARS-CoV-2 variant, as previously described[34,35]
237 (Supplementary Fig. 3A). Consistently, the amino acid sequences of all these variants from 834

238 to 863 aa are almost completely conserved, except for a single non-essential substitution at
239 position 856 only in BA.1.18 (Fig. 3B, Supplementary Fig. 3B). Thus, PA-001 showed an
240 advantage that was effective on broad range of naturally-occurring SARS-CoV-2 variants, in clear
241 contrast to the clinically-approved anti-S1 antibodies.
242
243 **PA-001 inhibits SARS-CoV-2 propagation and disease progression in vivo by either**
244 **pretreatment or posttreatment after virus infection**
245 We assessed the antiviral effect of PA-001 in infection animal models. We initially examined
246 the effect of prophylactic treatment with PA-001 before virus inoculation on propagation of
247 infectious SARS-CoV-2 in a Syrian hamster infection model[36,37] (Fig. 4A-a); Syrian hamsters
248 were pretreated with PA-001 at 0.3, 1.0, or 3.0 mg/kg, or saline as a vehicle control
249 intraperitoneally twice [at 12 and 2 h before virus inoculation (-0.5 and -0.08 day)], followed by
250 intranasal inoculation with SARS-CoV-2 (Delta variant), and then posttreatment with PA-001 at
251 the same concentrations three times [at 12, 24, and 36 h (0.5, 1, and 1.5 day)]. Hamsters were
252 sacrificed at day 2 for collecting lungs to quantify the infectious titer of SARS-CoV-2. SARS-
253 CoV-2 infectious titers detected in these tissues derived from vehicle-administered hamsters were
254 significantly reduced by PA-001 treatment in a dose-dependent manner, by up to 3.5-log (at 3.0
255 mg/kg of PA-001) (Fig. 4A-b). These data indicate the potential anti-SARS-CoV-2 effect of PA-
256 001 in hamsters by prophylactic treatment.
257 To further evaluate the therapeutic efficacy by posttreatment after infection, we examined the
258 pathogenicity induced by SARS-CoV-2 propagation in mice upon posttreatment with PA-001 after
259 infection; BALB/cCrSlc mice intranasally infected with a mouse-adapted SARS-CoV-2 (QHmusX
260 strain)[38] were treated intraperitoneally with PA-001 at 10 or 30 mg/kg, saline as a vehicle control,
261 or CAS + IMD as a positive control at 1, 8, 24, 48, 72, and 96 h after virus inoculation (0.04, 0.3,
262 1, 2, 3, and 4 days), and were chased to measure body weight as well as survival rate daily up to
263 day 10 (Fig. 4B-b, c). Seven mice out of eight treated with the vehicle were dead or reached the
264 humane endpoint (survival rate = 12.5%) at day 6, and body weights of vehicle-treated mice were
265 gradually decreased following SARS-CoV-2 infection to 73-80% of the original until day 5 (Fig. 4B-
266 b, c). In contrast, all mice treated with PA-001 after virus inoculation at either 10 or 30 mg/kg
267 survived (survival rate = 100%), whereas one mouse was dead upon CAS + IMD treatment
268 (survival rate = 87.5%) (Fig. 4B-b). Furthermore, PA-001-treated group showed only a transient
269 body weight reduction by up to around 11 % at day 3, followed by a recovery to the original body
270 weight level at day 10, as the case with CAS + IMD-treated mice (Fig. 4B-c).
271 We further examined histopathology in the lung as well as body weight and SARS-CoV-2 viral
272 load in the lung in Syrian hamsters posttreated with PA-001 after SARS-CoV-2 infection (Fig. 4C);
273 Hamsters after intranasal SARS-CoV-2 infection were posttreated with PA-001 (1 or 5 mg/kg) or
274 saline at 2, 8, 24, 48, and 72 h and were collected at day 5 to analyze histopathology and viral
275 RNA levels in the lung as well as chased for measuring body weight up to day 5 (Fig. 4C-a).

Body weight loss induced by SARS-CoV-2 propagation (to 88% in the vehicle-control group) was significantly recovered by PA-001 posttreatment (to 94% in PA-001-treated group) (Fig. 4C-b). SARS-CoV-2 RNA levels in the lung were reduced by PA-001 treatment in a dose-dependent manner by up to 1.6-log reduction (by 5.0 mg/kg of PA-001) (Fig. 4C-c). Histopathological examination revealed severe pneumonia with consolidation from vehicle-treated hamsters, whereas such severe illness in histopathology was improved by PA-001 treatment, especially at 5 mg/kg (Fig. 4C-d). Thus, PA-001 inhibited SARS-CoV-2 propagation in the lung and suppressed the resultant disease progression by post-treatment after infection in mice and hamsters.

Combination treatment with PA-001 and remdesivir augments the antiviral effects

Combination treatment with multiple drugs with different mode of action generally enhances the antiviral effect and decreases the risk for selecting drug-resistant variants[39]. We then examined the combination treatment of PA-001 with RDV at various concentrations to evaluate the antiviral effects in cell-based infection assay. As shown in Fig. 5A, RDV reduced SARS-CoV-2 production in a dose-dependent manner by single treatment, and this RDV's antiviral effects were enhanced by addition of PA-001 (Fig. 5A): e.g., RDV at 1,500 nM and PA-001 at 0.70 nM single treatment reduced viral production to 51% and 43%, respectively, but combination with RDV at 1,500 nM plus PA-001 at 0.70 nM decreased viral production to 11% of the control (Fig. 5A), indicating that PA-001 potentiated the antiviral activity of RDV.

We next examined the effect of combination therapy with PA-001 and GS-441524 (RDV-m), the active metabolite of RDV[40], in SARS-CoV-2 infection mouse model. BALB/cCrSlc mice intranasally inoculated with a mouse-adapted SARS-CoV-2 strain were intraperitoneally treated with RDV-m (25, 12.5, 12.5 mg/kg), RDV-m (25, 12.5, 12.5 mg/kg) + PA-001 (26 mg/kg), or vehicle control (Fig. 5B-a). The vehicle-control group mice showed a continuous decrease in body weight and all the mice died or reached the humane end point at day 5 after infection (Fig. 5B-b, c, black). In contrast, body weight loss of mice treated with RDV-m alone was only transient until day 3 to 4, followed by a gradual recovery, with all the mice survived until day 10 (Fig. 5B-b, c, blue). Consistently, virus infectious titer in the lung was significantly decreased by 1.2-log, although the lung weight, as a marker of tissue damage and inflammation was not significantly improved by single treatment with RDV-m (Fig. 5B-d, e). Combination treatment with RDV-m and PA-001 more rapidly recovered the body weight loss at day 4 to 7 compared with RDV-m single treatment, with no death during the whole experimental period (Fig. 5B-b, c, red), and showed additional reduction in SARS-CoV-2 infectious titer in the lung (by 1.8-log) (Fig. 5B-d, red). Furthermore, lung weight increase by SARS-CoV-2 was significantly improved by RDV-m + PA-001 cotreatment (Fig. 5B-e, red).

We further examined the production profile of cytokines and chemokines, especially those reportedly associated with the COVID-19 severe disease progression, including interleukin (IL)-6,

314 tumor necrosis factor-alpha (TNF-α), IL-1β, granulocyte colony stimulating factor (GCSF),
315 interferon (IFN)-γ, IFNγ-induced protein 10 (IP10), macrophage inflammatory protein 1-alpha
316 (MIP-1α), and monocyte chemoattractant protein-1 (MCP1)[41-44], in both the serum and the lung
317 of mice at day 3 postinfection. As shown in Fig. 5C, SARS-CoV-2-induced production of IL-6,
318 TNF-α, IL-1β, IP-10, MIP-1α, and MCP-1 at least either in the serum or the lung was significantly
319 inhibited by RDV-m monotreatment, and most of these expressions were more remarkably
320 reduced by combination treatment with RDV-m and PA-001 (Fig. 5C). Furthermore, induction of
321 IP-10 in serum was significantly reduced in PA-001 and RDV-m combination treatment from RDV-
322 m single treatment; Production of TNF-α and IFN-γ in the serum was significantly reduced under
323 only combination treatment with PA-001 and RDV-m, but not single treatment with RDV-m (Fig.
324 5C). Thus, combination treatment with PA-001 potentiated the anti-SARS-CoV-2 effect of RDV
325 and the resultant disease progression.
326
327 **Pharmacokinetics and safety of PA-001 in healthy volunteers**
328 A double-blind, randomized, placebo-controlled phase I study for PA-001 was conducted in 2
329 parts (Part A and B) to examine the safety, tolerability, and pharmacokinetics of PA-001 in healthy
330 volunteers.
331 Part A was a single-dose sequential-group study with a total of 32 randomized participants.
332 Baseline characteristics were balanced across cohorts, in which mean age of participants was 47
333 years (range 22–75 years) and the majority of participants were female (59.4%), white (65.6%),
334 and not Hispanic or Latino (62.5%), with a mean BMI of 26.17 kg/m^2 (Fig. 6A). These volunteers
335 were grouped into five cohorts who were administered intravenously with a single administration
336 of either i) placebo (n = 8), ii) 18 mg PA-001 (n = 6), iii) 64 mg PA-001 (n = 6), or iv, v) 128 mg PA-
337 001 (n = 6 to younger and n = 6 to elderly). Administration with PA-001 at 128 mg had two
338 cohorts, one with younger (median age of 37.2 years, iv) and one with elder volunteers (median
339 age of 69.8 years, v). These cohorts were chased to observe adverse effects as well as to collect
340 the plasma in a time course up to 48 h post-administration for measuring the concentration of PA-
341 001. As a result, PA-001 was well-tolerated, showing no severe adverse effects related with
342 treatment (treatment emergent adverse effects, TEAEs) in all individuals (Fig. 6B and
343 Supplementary Table 4A). Observed events were mild, including headache (1 subject in Placebo,
344 2 subjects in 64 mg PA-001) and vomiting (1 subject in 64 mg PA-001) (Fig. 6B and Supplementary
345 Table 4A). Pharmacokinetics profiles were presented with plasma concentrations against the
346 time course up to 48 h after single dosing (Fig. 6C), and pharmacokinetic parameters of PA-001
347 at each dose calculated based on these profiles (Fig. 6D and Supplementary Table 5). Dose
348 proportional increases in the peak concentrations and exposures of PA-001 were observed across
349 the evaluated dose range (Fig. 6C). PA-001 was readily detectable in plasma at 0.5 h after
350 administration with an average maximal concentrations (C_{max}) of up to 18,300 ng/mL (9,610 nM)
351 at 128 mg treatment, and was gradually declined, with 3.61-4.79 h as half-life ($T_{1/2}$). Given the

352 IC_{50} of 0.93-2.2 nM in the cell-based infection assay against the Omicron strains, BA.1.18 and
353 XBB.1.16 (Supplementary Table 3), 128 mg PA-001 group exhibited more than 4,300-10,300-fold
354 concentration of IC_{50} in plasma at peak (C_{max}) at 1 h after administration (Fig. 6C). The overall
355 exposure of PA-001 ($AUC_{0\text{-tlast}}$) was up to 74,200 ng·h /mL at 128 mg administration (younger).
356 Part B was a multi-dose sequential-group study, in which total 15 participants were randomized
357 into three groups who received multiple dosing of either placebo (n = 4), 64 mg PA-001 (n = 5), or
358 128 mg PA-001 (n = 6) once a day until day 5 (Supplementary Table 6). The mean age of
359 participants was 37 years (range 24–60 years); Eight (53.3%) males and seven (46.7%) females,
360 with a mean BMI of 27.29 kg/m^2. The majority (66.7%) of subjects were White (Supplementary
361 Table 6). Pharmacokinetics parameters on day 1 and day 5 (Supplementary Table 7) were
362 similar to those of single dosing in part A (Fig. 6D and Supplementary Table 5). Following
363 multiple doses of 64 and 128 mg for 5 days, $AUC_{0\text{-}\tau}$ and C_{max} increased in a supra proportional
364 manner with respect to dose. The AR_{AUC} (Accumulation ratio based on $AUC_{0\text{-}\tau}$) was 1.01 for the
365 64 mg dose level and 1.03 for the 128 mg dose level (Supplementary Table 7B). Because there
366 was no accumulation, steady state concentrations of PA-001 were achieved from the onset of the
367 multiple dosing period. No serious adverse effects related with multi-dosing of PA-001 was
368 observed, although seven (46.7%) subjects had at least 1 mild TEAE, of whom 2 received 64 mg
369 PA-001 (Grade 1), 4 received 128 mg PA-001 (3 of Grade 1, 1 of Grade 2), and 1 received placebo
370 (Grade 1) (Supplementary Table 4B). Three (20.0%) subjects had Grade 1 TEAE possibly
371 related to study treatment (2 received 64 mg, 1 received 128 mg), but all these TEAEs had
372 resolved by the end of the study (Supplementary Table 4B). There were no deaths, serious
373 adverse effects, or discontinuations because of adverse effects.
374 Thus, PA-001 provided the sustained plasma concentration in human individuals above those
375 required for antiviral activity, with preferable safety profiles.
376
377
378 **Discussion**
379 In this study, we identified a 13-amino acid macrocyclic peptide, PA-001, specifically binding to
380 FPPR on the S2 subunit of the SARS-CoV-2 Spike protein, which has not been targeted by
381 antibodies or antiviral agents so far. Despite extensive efforts of cryo-EM analysis, we were
382 unable to obtain a high-resolution structure of the PA-001/Spike complex, probably due to the
383 characteristic of FPPR, having high conformational flexibility, as mentioned below[7,45,46].
384 Alternatively, to demonstrate the binding site, we created SARS-CoV-2 variants more than 100-
385 fold resistance to PA-001 and found an amino acid substitution cluster within residues 836-862,
386 which resides at FPPR, upstream of FP. Mutations in this region completely abolished Spike's
387 capacity to bind to PA-001, confirming this segment as the PA-001-binding site. In the pre-fusion
388 form, FPPR is positioned on the surface of Spike trimer between the convex CTD1 and CTD2,
389 forming a shallow depression at the surface. FPPR is suggested to control the RBD movement

390 between its up and down conformations[4]: FPPR is structured and clamps RBD in the down
391 conformation of the pre-fusion form through interaction of Asp614 (in RBD) with Lys854 (in FPPR),
392 whereas it moves out and unstructured in the RBD down conformation[4,47-49]. Upon ACE2-RBD
393 engagement and the following S1 release, FPPR, together with the adjacent FP, undergoes an
394 overall translocation during the conformational rearrangement to be positioned at the top of the
395 S2 trimer and form a cone-shaped structure, which functions to be inserted into the target cellular
396 membrane. The binding of PA-001 to FPPR at the pre-fusion form (Fig. 2A and F) would
397 sterically interfere with this mobility of FPPR toward the formation of the cone-shaped structure
398 (intermediation form; Supplementary Fig. 1) that is required for the fusion process. These
399 findings highlight FPPR as a previously unexplored but potential target for antiviral drug
400 development.
401 Previously developed Spike-targeting therapeutics largely act through antibodies directed
402 against S1 such as casirivimab and imdevimab, amubarvimab and romlusevimab, bamlanivimab,
403 bamlanivimab and etesevimab, sotrovimab, tixagevimab and cilgavimab, and bebtelovimab[14,15].
404 These antibodies primarily exert anti-SARS-CoV-2 activity by neutralization of infection through
405 blocking Spike-ACE2 interaction and/or by engaging Fc-mediated effector functions that promote
406 viral clearance. However, their neutralization activity has been severely impaired or completely
407 lost by accumulated mutations in RBD of the S1 subunit among the recent Omicron sublineages.
408 The NTD in S1, another target of antibodies, also has high sequence variability. In contrast, the
409 S2 region is more conserved in sequence and represents a target for developing broadly active
410 antivirals. S2-targeting antibodies reported so far mainly recognize the region downstream of
411 the S2′ site (residues 811-825, previously referred to as FP, but recently considered an
412 intermediate loop) or the stem helices upstream of HR2, however, they had relatively modest
413 antiviral potency, likely due to the limited surface accessibility by antibodies as well as low
414 immunogenicity[17,50,51]. To overcome such limitations, non-antibody modalities have been
415 applied so far, such as peptides and aptamers, which have smaller molecular size that can bind
416 to regions inaccessible to conventional antibodies. HR2-mimetic peptides, such as EK1 and
417 HY3000, designed to interfere with the HR1-HR2 interaction during the conformational change to
418 the post-fusion form, have shown broad antiviral activity across SARS-CoV-2 variants, with
419 reported original IC_{50} at 500-3,000 nM, and their activities were further optimized through the lipid
420 conjugation[17,18]. S2-targeting DNA aptamers have also been reported, though most of their
421 antiviral activities in infection models remains to be characterized[52]. Among all these S2-directed
422 agents, PA-001 exhibited one of the most potent anti-SARS-CoV-2 activities reported to date (IC_{50}
423 = 0.23–2.9 nM of PA-001 v.s. 2468 nM of EK1[18] and 580 nM of HY3000[20]. The second key
424 characteristics of PA-001 lies in its target region, FPPR, as a highly conserved region with minimal
425 variations. The third notable feature of PA-001 is its 13-residue macrocyclic structure, markedly
426 smaller than the previously reported mimicking peptides mentioned above (typically more than 30
427 residues), making it accessible to FPPR positioned in shallow depression at the surface of Spike

428 pre-fusion form. In addition, its cyclic architecture generally confers improved proteolytic stability,
429 reduced immunogenicity, and favorable pharmacokinetics.
430 So far, macrocyclic peptides have been applied to target SARS-CoV-2 Spike to develop anti-
431 SARS-CoV-2 agents, majority of which target RBD in S1[53-57]. Among them, in vivo anti-SARS-
432 CoV-2 effect was shown for three series of peptides, 6L3-1F3P11hR (against RBD), multivalent
433 bicyclic peptides (against RBD), and S-20-1 (targeting both RBD and HR1)[54,56,57]. However,
434 antiviral activity of S-20-1 was relatively mild, with 540-10,230 nM as IC_{50} in cell-based infection
435 assay, and that of 6L3-1F3P11hR varied at 1-332 nM depending on the target SARS-CoV-2
436 variants, consistent with the property of RBD-targeting agents. None of them have been
437 reported to be administered in human. In addition to its distinct target (FPPR), PA-001 shows an
438 advantage among these macrocyclic peptides with its high activity in vivo and administration
439 profile in human.
440 In infection mouse and hamster models, PA-001 effectively inhibited SARS-CoV-2-induced
441 disease progression when administered before or after infection, underscoring its potential for
442 both prophylactic and therapeutic use. Additionally, combination treatment with PA-001 with
443 RDV elevated therapeutic profiles, highlighting its well compatibility with already-approved
444 antivirals. This is consistent with that PA-001 has a distinct mode of action from those of any
445 clinically approved anti-SARS-CoV-2 agents so far. Given the demand for effective anti-COVID-
446 19 therapies, especially for immunocompromised patients who respond poorly to current
447 treatments and evolve drug-resistance[1-3], peptide-based antivirals with different mode of action
448 would provide an additional choice for COVID-19 therapy. Encouragingly, phase I clinical trial of
449 PA-001 in 32 healthy volunteers demonstrated well tolerability (up to 128 mg administration of PA-
450 001) without serious adverse events, regardless of age. In the single-dose cohort, the C_{max}
451 reached 18,300 ng/mL [9,610 nM, more than 4,300-fold higher than IC_{50} (0.93–2.2 nM) against
452 Omicron variants] with half-life of 4.46 h, and drug exposure was sufficient to maintain
453 concentrations above the cellular IC_{50} for up to 24 h post-dose in Groups of 128 mg administration.
454 Collectively, these findings suggest that PA-001 achieves robust and sustained systemic exposure,
455 supporting a favorable pharmacokinetic profile. Therefore, our data raise PA-001 as a promising
456 anti-SARS-CoV-2 drug that targets S2 and inhibits fusion process, and forthcoming clinical trials
457 will assess its efficacy in SARS-CoV-2-infected patients.
458 In summary, our study shows the usefulness of macrocyclic peptides as a potential therapeutic
459 modality against COVID-19, that demonstrates FPPR in the S2 region as a druggable target to
460 inhibit virus fusion process. The strong antiviral potency warrants PA-001 as a candidate seed
461 for the development of an anti-SARS-CoV-2 fusion inhibitor.
462
463

464 **Methods**

465 **Synthesis of PA-001**

466 PA-001 was synthesized using standard Fmoc solid-phase peptide synthesis (SPPS), as
467 described in the Supplementary Notes. After coupling of all amino acids, the N-terminus was
468 deprotected and subsequently chloroacetylated on resin, followed by global deprotection using a
469 standard deprotection cocktail containing trifluoroacetic acid (TFA). The linear peptide was
470 precipitated by the adding the deprotection solution to more than a 10-fold excess of diethyl ether
471 and hexane. The resulting crude peptide pellet was resuspended in diethyl ether and re-pelleted
472 three times. After the final wash, the pellet was dried and dissolved in DMSO/H_2O, followed by
473 the addition of triethylamine to induce intramolecular cyclization via thioether bond formation
474 between the cysteine thiol and the N-terminal chloroacetyl group. Upon completion of cyclization,
475 the cyclic peptide was purified by standard reverse-phase HPLC. The molecular mass was
476 confirmed by single-quadrupole LC/MS (LCMS-2020 system, Shimadzu).

477

478 **Cell culture**

479 VeroE6/TMPRSS2 cells, a VeroE6 cell line overexpressing transmembrane protease, serine 2
480 (TMPRSS2) and highly susceptible to SARS-CoV-2 infection[25], were cultured in Dulbecco's
481 modified Eagle's medium (DMEM; Life Technologies) supplemented with 10% fetal bovine serum
482 (FBS; Cell Culture Bioscience), 10 units/mL penicillin, 10 mg/mL streptomycin, 10 mM HEPES
483 (pH 7.4), and 1 mg/mL G418 (Nacalai) at 37°C in 5% CO_2. During the infection assay, 10% FBS
484 was replaced with 2% FBS, with removing G418. HEK293T cells were cultured in DMEM
485 supplemented with 10% FBS (heat-inactivated) and 50 μg/mL gentamicin at 37°C in 5% CO_2.

486

487 **Reagents**

488 Anti-SARS-CoV-2 Spike S1 antibodies, casirivimab (CAS) and imdevimab (IMD), were cloned
489 into human IgG1 and kappa expression vectors and co-transfected into Expi293F cells (Thermo
490 Fisher Scientific) as described previously[58]. Mutant spike proteins were generated by
491 introducing substitutions into expression vectors coding codon-optimized spike trimeric protein[59]
492 by PCR, and expressed with Expi293F cells. Antibodies and mutant spike proteins were purified
493 from the culture supernatant using Protein G columns (Thermo Fisher Scientific) and TALON
494 columns (Clontech), respectively, and dialyzed against PBS. Nucleotide analogs, RDV and its
495 active metabolite, GS-441524 (RDV-m), were purchased from Chemscene Inc (CS-0028115) and
496 Cayman Chemical (30469), respectively. PA-001 and HA tagged PA-001 were produced by
497 PeptiDream Inc. DMSO was purchased from Sigma-Aldrich. Mefloquine was purchased from
498 Tokyo Chemical Industry.

499

500 **Cell-based infection assay**

501 SARS-CoV-2 was handled in a biosafety level 3 (BSL3). We used the SARS-CoV-2 Wk-521

502 (Wuhan type), QK002 (Alpha), TY8-612 (Beta), TY7-503 (Gamma), TY11-927 (Delta), TY38-873
503 (Omicron; BA.1.18), and TY41-984 (Omicron; XBB.1.16) strains, clinical isolates from a COVID-
504 19 patient[25]. Virus infectious titers were measured by inoculating cells with a 10-fold serial
505 dilution of virus and cytopathology measured to calculate $TCID_{50}$/mL[25]. For the infection assay,
506 VeroE6/TMPRSS2 cells were inoculated with virus at an MOI of 0.003 for 1 h and washed to
507 remove unbound virus. Cells were cultured for an additional 24, 36, and 48 h prior to detection
508 of extracellular viral RNA or intracellular viral N protein (24 or 36 h), and cytopathic effects (CPE)
509 (48 h), respectively. Compounds were added during virus inoculation (1 h) and incubation after
510 washing (24, 36, or 48 h), or incubation after washing only.
511
512 **Isolation and quantification of viral RNA**
513 Viral RNA was extracted with RNeasy mini kit (QIAGEN) from cells and MagMax
514 Viral/Pathogen II Nucleic Acid Isolation kit (Thermo Fisher Scientific) or QIAamp Viral RNA mini
515 kit (QIAGEN) from culture supernatant. Viral RNA was quantified by real time RT-PCR analysis
516 with a one-step qRT-PCR kit (THUNDERBIRD Probe One-step qRT-PCR kit, TOYOBO) using 5'-
517 ACAGGTACGTTAATAGTTAATAGCGT-3', 5'- ATATTGCAGCAGTACGCACACA-3' as a primer
518 set, and 5'-FAM-ACACTAGCCATCCTTACTGCGCTTCG-TAMRA-3' (E-set) as a probe[60].
519
520 **Detection of viral proteins**
521 Viral proteins were detected using rabbit anti-SARS-CoV N antibody[61] and mouse anti-SARS-
522 CoV-2 spike antibody (abcam, ab273433) as primary antibodies, with anti-rabbit IgG-HRP (Cell
523 Signaling, 7074) and anti-mouse IgG-HRP (Cell Signaling, 7076) as secondary antibodies by
524 immunoblot analyses as previously reported[62].
525
526 **Virus-cell binding assay**
527 SARS-CoV-2 preincubated with the indicated compounds for 30 min was exposed to
528 VeroE6/TMPRSS2 cells at an MOI of 0.01 at 4°C for 15 min. After extensive wash, total RNA
529 was extracted from cells and viral RNA was quantified by real time RT-PCR to measure cell-bound
530 virus, as described [63].
531
532 **PA-001-Spike binding assay**
533 Binding of HA-tagged PA-001 to SARS-CoV-2 Spike proteins was quantified by ELISA as
534 follows: Recombinant wild type (from Sino biological, 40589-V08B1, 40591-V08B1, and 40590-
535 V08B) or mutated Spike proteins were immobilized on the plates, and then incubated with PA-
536 001-HA at various concentrations together with or without excess amount of non-tagged PA-001,
537 used as a binding competitor. After washing with PBST, horseradish peroxidase-labeled mouse
538 anti-HA tag antibody (MBL Life Science, M180-7, 1:5000 or 1:2500) was added, and visualized
539 with reacting with a substrate solution (SUMITOMO BAKELITE) to detect absorbance at 450 nm

540 with a microplate reader (TECAN).
541
542 **Cell membrane fusion assay**
543 The S-ACE2 interaction-mediated cell-cell fusion assay was performed essentially based on
544 the previous report[29], with some modifications. Spike proteins expressed in HEK293T cells
545 mediate the fusion with VeroE6/TMPRSS2 cells, and the cell-cell fusion was quantified based on
546 the measurement of luminescence intensity derived from reconstituted NanoLuc reporter
547 (composed of HiBiT stably expressed in VeroE6/TMPRSS2 cells and LgBiT transiently expressed
548 in HEK293T cells). HEK293T cells were co-transfected with the plasmid expressing Spike in
549 combination with the HaloTag-inserted pBiT1.1-N[TK/LgBiT] plasmid (Promega) using
550 Lipofectamine 3000 Transfection Reagent according to the manufacturer's instruction (Thermo
551 Fisher Scientific). At 48 h post-transfection, the cells were co-incubated with
552 VeroE6/TMPRSS2/HiBiT cells in the presence or absence of varying concentrations of PA-001 for
553 1 h. The media were replaced with Opti-MEM containing 0.5% FBS and the substrate of
554 NanoLuc from Nano-Glo Live Cell Assay System (Promega) to measure luminescence.
555
556 **Generation of PA-001 resistant viruses**
557 To obtain PA-001-resistant SARS-CoV-2 variants, SARS-CoV-2 (WK-521) was inoculated to
558 VeroE6/TMPRSS2 cells at an MOI of 0.003, followed by incubation of the cells in the presence of
559 1,000 nM PA-001 for 48 h and recovery of culture supernatant. The 1:1 diluted culture
560 supernatant was then inoculated to VeroE6/TMPRSS2 cells to repeat the same procedure until
561 the second passage. The 1:10 diluted culture supernatant was inoculated to the cells in the
562 presence of 10 μM PA-001, followed by recovery of culture supernatant at 24 h later, which was
563 repeated for the three additional passages. Virus was further amplified with two additional
564 passages in the absence of PA-001.
565
566 **SARS-CoV-2 pseudovirus infection assay**
567 SARS-CoV-2 pseudoviruses were produced using vesicular stomatitis virus (VSV)-based
568 pseudovirus system, using the expression plasmid for the G-deficient VSV carrying the luciferase
569 gene and that encoding SARS-CoV-2 Spike derived from the Wuhan type Wk-521 or the Omicron
570 sublineages, JN.1 or XFG, essentially as previously described[64,65]. VeroE6/TMPRSS2 cells
571 were inoculated with the SARS-CoV-2 pseudovirus in the presence or absence of various
572 concentrations of the indicated compounds, peptide, or antibodies followed by incubation with or
573 without the compounds, peptide, or antibodies for 24 h to measure intracellular luciferase activity
574 with Luciferase Assay System (Promega), as described[62].
575
576 **Sequence analysis of PA-001 resistant viruses**
577 cDNA libraries were generated from RNA extracted from SARS-CoV-2 isolates according to

578 the ARTIC nCoV-2019 sequencing protocol v3 (LoCost) (https://www.protocols.io/view/ncov-
579 2019-sequencing-protocol-v3-locost-bp2l6n26rgqe/v3). Whole-genome sequencing was
580 performed using the MinION platform (Oxford Nanopore Technologies), followed by consensus
581 sequence generation using the Medaka pipeline (https://github.com/nanoporetech/medaka).
582 Lineage and clade assignments, as well as mutation identification, were conducted using the
583 Pangolin COVID-19 Lineage Assigner (https://pangolin.cog-uk.io/) and Nextclade
584 (https://clades.nextstrain.org/).
585
586 **Pharmacokinetic analysis of PA-001 in mice**
587 The study was conducted under accreditation by the Association for Assessment and
588 Accreditation of Laboratory Animal Care (AAALAC) with approval of Institutional Animal Care and
589 Use Committee (IACUC, protocol No. PK-T-07182021). Fasted female BALB/c mice (8 weeks
590 old, Si Bei Fu Laboratory Animal Technology) were intraperitoneally administered with PA-001 at
591 the dose of 10 mg/kg, and were sacrificed to collect blood at 1, 7, and 24 h post-administration.
592 The blood was centrifuged to prepare plasma, mixed with acetonitrile containing formic acid, and
593 centrifuged. The supernatant was injected onto LC/MS/MS system (LCMS-8060, Shimadzu) to
594 determine plasma concentrations of PA-001.
595
596 **SARS-CoV-2 infection in vivo**
597 For infection to the mouse model in Fig. 4B and Fig. 5B and C, all the experiments were
598 approved by the Animal Care and Use Committee of the National Institute of Infectious Diseases
599 in Japan, and handled in BSL3 animal facilities (ABSL3) that were certified by the Japan Health
600 Sciences Foundation according to the guidelines of this committee. BALB/c mice (13 weeks old,
601 female, Japan SLC) were maintained for 3 weeks in the specific pathogen-free facility and then
602 transferred to the ABSL3. After a week of acclimation to the facility, the mice (17 weeks old)
603 were anesthetized by intraperitoneal injection with a mixture of 0.1 ml/10 g body weight of 1.0 mg
604 ketamine and 0.02 mg xylazine. Animals were then inoculated intranasally with 3 x 10^3 $TCID_{50}$
605 (30 μl, 5 LD_{50}/mouse, 100% lethal dose) QHmusX, a mouse-adopted SARS-CoV-2 clone[38].
606 Body weight was measured daily for 10 days (n = 10–11 per group), and animals were sacrificed
607 at 3 and 10 days post-inoculation to analyze viral replication, cytokine expression, and disease
608 pathology (n = 4 or 6–7 per group). Clinical signs were observed up until 10 days post-
609 inoculation. The humane endpoint was defined as the appearance of clinically diagnostic signs
610 of respiratory stress, including respiratory distress and more than 25% weight loss. Animals
611 were euthanized under anesthesia with an overdose of isoflurane if severe disease symptoms or
612 weight loss were observed. In Fig. 4B, PA-001 was administered intraperitoneally at a dose of
613 10 or 30 mg/kg, at 0.04, 0.3, 1, 2, 3, and 5 days post-inoculation. The CAS + IMD-treatment
614 group received the cocktail CAS + IMD antobodies (10 mg/kg) at 1 h post-inoculation. The
615 vehicle control group was administered with PBS. In, Fig. 5B and C, RDV-m was administered

616 intraperitoneally at a dose of 25 mg/kg (on day 1 post-infection) and 12.5 mg/kg (on days 2 and 3
617 post-infection), with a volume of 6.25 mL/kg per dose, once daily. Concurrently, PA-001 was
618 administered intraperitoneally at a dose of 26 mg/kg, with a volume of 10 mL/kg per dose, once
619 daily. The control group was administered with PBS.
620 Infection studies to the hamster model shown in Fig. 4A and C were conducted in the animal
621 BSL-3 laboratory, accredited by AAALAC, under IACUC-approved protocol (22-032, 16103.01).
622 In Fig. 4A, seven-week-old male Syrian hamsters (Envigo) were intranasally inoculated with 3.48
623 x 10^3 $TCID_{50}$ of SARS-CoV-2 (Delta variant, BEI Resources, NR-56116) under anesthesia with
624 ketamine/xylazine at day 0. PA-001 was intraperitoneally administered to hamsters twice daily
625 at 0.3, 1, or 3 mg/kg, or PBS as a vehicle control, at 12 h and 2 h prior to infection and 12 h, 24 h,
626 and 36 h following infection (-0.5, -0.08, 0.5, 1, and 1.5 day post infection). Lung in the hamsters
627 were collected at 2 days post-infection to examine the infectious titer of SARS-CoV-2. In Fig. 4C,
628 Syrian Golden hamsters (female, 8 week-old, Charles Reiver Laboratories) were intranasally
629 infected with 2.11 x 10^5 $TCID_{50}$ SARS-COV2 (USA_WA1/2020, CDC, kindly provided by UTMB
630 Galveston), and then administered intraperitonially with either PBS as a vehicle control or PA-001
631 1 or 5 mg/kg (n=6/group) (7.5 mL/kg) at 2, 8, 24, 48 and 72 h post-infection. Body weight and
632 clinical observation were evaluated every day, and the lungs were collected at five day
633 postinfection. The left lung lobes were used for quantifying SARS-CoV-2 RNA by real time RT-
634 PCR, whereas the right lung lobes were fixed with 10% neutral buffered formalin for
635 histopathological evaluation.
636
637 **Viral titration from mouse and hamster tissues**
638 Lung tissue samples from BALB/c mice were collected at the time of postmortem examination
639 and stored at -80°C. Tissue homogenates (10% w/v) were prepared in Dulbecco's Modified
640 Eagle medium (DMEM) containing 2% FBS, 50 IU/ml penicillin G, and 50 µg/ml streptomycin, and
641 samples were inoculated onto VeroE6/TMPRSS2 cell cultures, which were then examined for
642 observing cytopathic effects (CPEs) for 5 days to determine the viral infectivity titers ($TCID_{50}$) as
643 described above.
644 Lung tissue samples from Syrian hamsters were homogenized and centrifuged to collect the
645 supernatant. VeroE6/TMPRSS2 cells were treated with the supernatant to evaluate CPEs for 4
646 days to determine the viral infectivity titers with the Read-Muench formula[66].
647
648 **Detection of inflammatory cytokines and chemokines**
649 Homogenized mouse lung tissue samples (10% w/v) were diluted 1:1 in cell extraction buffer
650 [10 mM Tris (pH 7.4), 100 mM NaCl, 1 mM EDTA, 1 mM EGTA, 1 mM NaF, 20 mM $Na_4P_2O_7$, 2
651 mM Na_3VO_4, 1% Triton X-100, 10% glycerol, 0.1% SDS, and 0.5% deoxycholate (BioSource
652 International, Camarillo, CA)], incubated for 10 min on ice with vortexing, irradiated for 10 min with
653 UV-C light to inactivate infectious virus. Cytokine and chemokine levels were measured with

mouse cytokine–chemokine magnetic bead panel 96-well plate assay kit (Milliplex MAP kit, Merck Millipore), detected on a Luminex 200 instrument with xPONENT software (Merck Millipore), according to the manufacturer's instruction.

Phase I study

1. Study design and oversight

This phase I, double-blind, randomized, placebo-controlled, single- and multiple-ascending dose study of the safety, tolerability, and pharmacokinetics in healthy and elderly subjects was conducted at a single clinical site, Fortrea Clinical Research Unit Inc. The protocol (PA-001-101) was approved by Salus institutional review board (IRB). Study began in Sep 2024 and was completed in Jun 2025 (from FSFV to LPLV). All participants provided written informed consent before enrollment.

2. Study Design

This study was conducted in 2 parts of Part A and B, as shown below.

Part A comprised a single-dose, sequential-group study of PA-001. A total of up to 40 subjects were planned to be studied in up to 4 groups (Groups A1-4, PA-001 doses were 18, 64, 128 and 128 mg, respectively, with each group comprising 8 subjects. In each group, 6 subjects were to receive a single dose of PA-001 and 2 subjects were to receive a single dose of placebo. Age range was 18 to 65 years for Group A1-3, and >65 years for Group A4. Doses of PA-001 or placebo were administered in accordance with a randomization schedule on the morning of Day 1, after a fast of at least 10 h. Sentinel dosing: Groups A1 to A4 were divided into 2 subgroups, with each subgroup being dosed at least 24 h apart. The first subgroup comprised 2 subjects, with 1 subject receiving PA-001 and 1 subject receiving placebo. The second subgroup comprised 6 subjects, with 5 subjects receiving PA-001 and 1 subject receiving placebo. Continuation to dose the remaining 6 subjects was at the investigator's discretion.

Part B comprised a multiple-dose, sequential group study. Part B was permitted to start after completion of Group A3 (in Part A), at a dose level less than or equal to that administered in Groups A1 to A3. A total of 16 subjects were planned to be studied in 2 groups, with each group comprising 8 subjects. In each group, 6 subjects were to receive PA-001, and 2 subjects were to receive placebo once per day until day 5. PA-001 or placebo were administered in accordance with a randomization schedule after a fast of at least 10 h.

Inclusion criteria and exclusion criteria were described in Supplementary Notes.

3. Safety assessments

The condition of each subject was monitored from the time of signing the ICF to final discharge from the study. Subjects were observed for any signs or symptoms and asked about their condition by open questioning, such as "How have you been feeling since you were last asked?" at least once each day while resident at the study site and at each study visit. Subjects were also encouraged to spontaneously report adverse effects occurring at any other time during the

692 study. All nonserious adverse effects, whether reported by the subject voluntarily or on
693 questioning, or noted on physical examination, were recorded from initiation of study treatment
694 until study completion. Serious adverse effects were recorded from the time the subject signs
695 the ICF until study completion. The nature, time of onset, duration, and severity were
696 documented, together with an investigator's (or designee's) opinion of the relationship to study
697 treatment. Adverse events recorded during the study will be followed up, where possible, until
698 resolution or until the unresolved adverse effects were judged by the investigator (or designee) to
699 have stabilized. This was completed at the investigator's (or designee's) discretion.

700 **4. Administration**

701 In Part A, subjects received a single 50mL intravenous infusion over 1 h (± 2 min) containing
702 18 mg (Group A1), 64 mg (Group A2), or 128 mg (Groups A3 and A4) of PA-001 or placebo on day
703 1. In part B, subjects received multiple 50mL intravenous infusions over 1 h (± 2 min) containing
704 64 mg (Group B1) or 128 mg (Group B2) of PA-001 or placeboonce per day on day 1 through 5,
705 inclusive.

706 **5. Analysis of PA-001 concentrations**

707 Concentration of PA-001 in plasma and urine samples was measured with liquid
708 chromatography tandem mass spectrometry (LC/MS/MS, QTRAP® 5500 System, SCIEX).

709

710 **Statistics and reproducibility**

711 Bar graphs are presented as mean ± standard deviation with individual data sets, and
712 experiments were repeated in at least triplicates or more unless indicated otherwise. In this study,
713 GraphPad Prism (v.10.5.0) was used for the ordinary one-way ANOVA followed by Dunnett's
714 multiple comparisons with control (Fig. 2C-a, Fig. 4A-b, and Fig. 4C-c) or followed by tukey's
715 multiple comparisons (Fig. 5B-d, e, and C-a, b), and the ordinary two-way ANOVA followed by
716 Dunnett's multiple comparisons with control (Fig. 4B-c, Fig. 4C-b) or followed by tukey's multiple
717 comparisons (Fig. 2F-b and Fig. 5B-c).

718

719 **Acknowledgments**

720 We appreciate Drs. Setsuo Hasegawa (Pharma Spur), Akihito Shimoi (SNBL), Takuma
721 Yonemura, Takeshi Chiyoda, Asuka Yamamoto (Sumida Hospital) for valuable scientific advice
722 based on clinical research experience, which contributed to the rationale for the starting dose in
723 the Phase I study. We also thank Dr. Keiichi Masuya for PA-001 generation. We are grateful to
724 Drs. Dai Izawa, Midori Ozaki, Takiko Yoshida, for their technical assistance. We thank the
725 members of the Management Department of Biosafety and Laboratory Animals for support with
726 the BSL3 facility. We also appreciate leadership of Dr. Gene Voskuhl (Fortrea Clinical Research)
727 to operate Phase I study. This study was supported by Japan Agency for Medical Research and
728 Development (AMED) under grand numbers JP25fk0310525 (K.W.), JP23fk0108590 (K.W.),
729 JP25ak0101271 (K.W.), 25wm0325079 (K.W.), JP253fa727002 (N.Nagata, T.S.),

JP25wm0125008 (T.S.), JP25fk0108732 (T.S.), JP223fa627003 (T.S.), JP22fk0108521 (M.M.); JSPS/MEXT under KAKENHI grant numbers JP24K18457 (H.Ohashi), JP24K02290 (K.W.), JP25K21782 (K.W.), JP25K21767 (K.W.), JP25K02691 (K.W.); JST MIRAI program grant number JPMJMI22G1 (K.W.); Takeda Science Foundation (K.W.).

Author Contributions

Experimental systems were developed by M.O., T.S., N.Nagata and K.W. Compound screening was supervised by M.O. and P.C.R. M.O., K.N.,T.N., K.S.,N.Nakamura and J.Y. performed screening for lead compound of PA-001. M.O., K.M. and H.Kurasaki optimized peptides and identified PA-001. Molecular biological and cell-based experiments were performed by H.Ohashi, Y.H., K.Shionoya, T.K., H.Ogawa, and K.W. Animal experiments using mice were designed and performed by N.IY., N.Nagata, and H.Kitamura, and those using hamsters were designed and managed by T.K., K.N. and H.Kitamura. Peptide synthesis was performed by M.O., H.Kurasaki, K.N., T.N., J.Y., K.Sudo, N.Nakamura, and K.M. Non-clinical ADME analyses was conducted by K.Y., Y.S. and T.H. Preparing materials was managed by H.Kurasaki, S.M., T.M., T.H., and S.I. Experimental design was developed by N.Nagata, M.O., P.C.R., T.S., and K.W. Phase I clinical trial was designed and managed by S.I., N.K., and M.M. Original draft was written by H.Ohashi, N.Nagata, S.M., H.Kitamura, and K.W. with critical discussion by T.K, M.O., H.Kurasaki, N.IY., Y.H., S.M., K.Shionoya, K.N., T.N., J.Y., K.Sudo., N.Nakamura, K.M., H.Ogawa, K.Yoshida, Y.S., T.M., T.H., S.I., Y.T., N.K., P.C.R., M.M., and T.S. Fundings were acquired by H.Ohashi, M.M., T.S., N.Nagata, and K.W. The project was supervised by H.Kitamura and K.W.

Competing Interests

T.K., M.O., H.Kurasaki, K.N., T.N., J.Y., K.Sudo, N.Nakamura, K.M., H.Ogawa, K.Y., Y.S., T.M., T.H., S.I., N.K., H.Kitamura and M.M. are employees of PeptiDream Inc. P.C.R. is CEO of PeptiDream Inc. M.M. is CMO of PeptiDream and CEO of PeptiAid Inc.

Data Availability

Source data are provided with this paper.

765 **References**

766 1 Iriyama, C. *et al.* Clinical and molecular landscape of prolonged SARS-CoV-2 infection with
767 resistance to remdesivir in immunocompromised patients. *PNAS Nexus* **4**, pgaf085 (2025).
768 2 Nooruzzaman, M. *et al.* Emergence of transmissible SARS-CoV-2 variants with decreased
769 sensitivity to antivirals in immunocompromised patients with persistent infections. *Nat*
770 *Commun* **15**, 7999 (2024).
771 3 Gandhi, S. *et al.* De novo emergence of a remdesivir resistance mutation during treatment of
772 persistent SARS-CoV-2 infection in an immunocompromised patient: a case report. *Nat*
773 *Commun* **13**, 1547 (2022).
774 4 Chen, B., Farzan, M. & Choe, H. SARS-CoV-2 spike protein: structure, viral entry and variants.
775 *Nat Rev Microbiol* **23**, 455–468 (2025).
776 5 Hoffmann, M. *et al.* SARS-CoV-2 Cell Entry Depends on ACE2 and TMPRSS2 and Is Blocked
777 by a Clinically Proven Protease Inhibitor. *Cell* **181**, 271–280 e278 (2020).
778 6 Shi, W. *et al.* Cryo-EM structure of SARS-CoV-2 postfusion spike in membrane. *Nature* **619**,
779 403–409 (2023).
780 7 Calvaresi, V. *et al.* Structural dynamics in the evolution of SARS-CoV-2 spike glycoprotein. *Nat*
781 *Commun* **14**, 1421 (2023).
782 8 Lei, R. *et al.* Functional and antigenic characterization of SARS-CoV-2 spike fusion peptide by
783 deep mutational scanning. *Nat Commun* **15**, 4056 (2024).
784 9 Shi, W. *et al.* Effect of the S2' site cleavage on SARS-CoV-2 spike. *Nat Commun* **16**, 11675
785 (2025).
786 10 Marcink, T. C. *et al.* Intermediates in SARS-CoV-2 spike-mediated cell entry. *Sci Adv* **8**,
787 eabo3153 (2022).
788 11 Xing, L. *et al.* Early fusion intermediate of ACE2-using coronavirus spike acting as an antiviral
789 target. *Cell* **188**, 1297–1314 e1224 (2025).
790 12 Grunst, M. W. *et al.* Structure and inhibition of SARS-CoV-2 spike refolding in membranes.
791 *Science* **385**, 757–765 (2024).
792 13 Dimitrov, D. S. Virus entry: molecular mechanisms and biomedical applications. *Nat Rev*
793 *Microbiol* **2**, 109–122 (2004).
794 14 Dong, M., Galvan Achi, J. M., Du, R., Rong, L. & Cui, Q. Development of SARS-CoV-2 entry
795 antivirals. *Cell Insight* **3**, 100144 (2024).
796 15 Chen, Y. *et al.* Broadly neutralizing antibodies to SARS-CoV-2 and other human coronaviruses.
797 *Nat Rev Immunol* **23**, 189–199 (2023).
798 16 Imai, M. *et al.* Efficacy of Antiviral Agents against Omicron Subvariants BQ.1.1 and XBB. *N*
799 *Engl J Med* **388**, 89–91 (2023).
800 17 Guo, L. *et al.* Targetable elements in SARS-CoV-2 S2 subunit for the design of pan-coronavirus
801 fusion inhibitors and vaccines. *Signal Transduct Target Ther* **8**, 197 (2023).
802 18 Xia, S. *et al.* Inhibition of SARS-CoV-2 (previously 2019-nCoV) infection by a highly potent

pan-coronavirus fusion inhibitor targeting its spike protein that harbors a high capacity to mediate membrane fusion. *Cell Res* **30**, 343–355 (2020).

19 Yan, W., Zheng, Y., Zeng, X., He, B. & Cheng, W. Structural biology of SARS-CoV-2: open the door for novel therapies. *Signal Transduct Target Ther* **7**, 26 (2022).

20 Sun, H. *et al.* Structural basis of HCoV-19 fusion core and an effective inhibition peptide against virus entry. *Emerg Microbes Infect* **9**, 1238–1241 (2020).

21 Vinogradov, A. A., Yin, Y. & Suga, H. Macrocyclic Peptides as Drug Candidates: Recent Progress and Remaining Challenges. *J Am Chem Soc* **141**, 4167–4181 (2019).

22 Ravel, G. *et al.* Additive effects of ALXN2420, a GH receptor antagonist, and octreotide on IGF1 suppression in vivo. *Eur J Endocrinol* **192**, 299–307 (2025).

23 Sun, D. *et al.* The discovery and structural basis of two distinct state-dependent inhibitors of BamA. *Nat Commun* **15**, 8718 (2024).

24 Brousseau, M. E. *et al.* Identification of a PCSK9-LDLR disruptor peptide with in vivo function. *Cell Chem Biol* **29**, 249–258 e245 (2022).

25 Matsuyama, S. *et al.* Enhanced isolation of SARS-CoV-2 by TMPRSS2-expressing cells. *Proc Natl Acad Sci U S A* **117**, 7001–7003 (2020).

26 Wang, M. *et al.* Remdesivir and chloroquine effectively inhibit the recently emerged novel coronavirus (2019-nCoV) in vitro. *Cell Res* **30**, 269–271 (2020).

27 Hansen, J. *et al.* Studies in humanized mice and convalescent humans yield a SARS-CoV-2 antibody cocktail. *Science* **369**, 1010–1014 (2020).

28 Jan, J. T. *et al.* Identification of existing pharmaceuticals and herbal medicines as inhibitors of SARS-CoV-2 infection. *Proc Natl Acad Sci U S A* **118** (2021).

29 Xia, S. *et al.* A pan-coronavirus fusion inhibitor targeting the HR1 domain of human coronavirus spike. *Sci Adv* **5**, eaav4580 (2019).

30 Matsuyama, S. *et al.* The Inhaled Steroid Ciclesonide Blocks SARS-CoV-2 RNA Replication by Targeting the Viral Replication-Transcription Complex in Cultured Cells. *J Virol* **95** (2020).

31 Li, G., Hilgenfeld, R., Whitley, R. & De Clercq, E. Therapeutic strategies for COVID-19: progress and lessons learned. *Nat Rev Drug Discov* **22**, 449–475 (2023).

32 Hoffmann, M. *et al.* The Omicron variant is highly resistant against antibody-mediated neutralization: Implications for control of the COVID-19 pandemic. *Cell* **185**, 447–456 e411 (2022).

33 Planas, D. *et al.* Considerable escape of SARS-CoV-2 Omicron to antibody neutralization. *Nature* **602**, 671–675 (2022).

34 Lu, Y., Ao, D., He, X. & Wei, X. The rising SARS-CoV-2 JN.1 variant: evolution, infectivity, immune escape, and response strategies. *MedComm (2020)* **5**, e675 (2024).

35 He, Q. *et al.* Neutralization of EG.5, EG.5.1, BA.2.86, and JN.1 by antisera from dimeric receptor-binding domain subunit vaccines and 41 human monoclonal antibodies. *Med* **5**, 401–413 e404 (2024).

36 Sia, S. F. *et al.* Pathogenesis and transmission of SARS-CoV-2 in golden hamsters. *Nature* **583**, 834–838 (2020).

37 Imai, M. *et al.* Syrian hamsters as a small animal model for SARS-CoV-2 infection and countermeasure development. *Proc Natl Acad Sci U S A* **117**, 16587–16595 (2020).

38 Iwata-Yoshikawa, N. *et al.* A lethal mouse model for evaluating vaccine-associated enhanced respiratory disease during SARS-CoV-2 infection. *Sci Adv* **8**, eabh3827 (2022).

39 Abdelnabi, R., Maes, P., de Jonghe, S., Weynand, B. & Neyts, J. Combination of the parent analogue of remdesivir (GS-441524) and molnupiravir results in a markedly potent antiviral effect in SARS-CoV-2 infected Syrian hamsters. *Front Pharmacol* **13**, 1072202 (2022).

40 Sheahan, T. P. *et al.* Broad-spectrum antiviral GS-5734 inhibits both epidemic and zoonotic coronaviruses. *Sci Transl Med* **9** (2017).

41 Zhang, Z. *et al.* Associations of immunological features with COVID-19 severity: a systematic review and meta-analysis. *BMC Infect Dis* **21**, 738 (2021).

42 Chen, L. D. *et al.* Association between cytokine profiles and lung injury in COVID-19 pneumonia. *Respir Res* **21**, 201 (2020).

43 Jontvedt Jorgensen, M. *et al.* Increased interleukin-6 and macrophage chemoattractant protein-1 are associated with respiratory failure in COVID-19. *Sci Rep* **10**, 21697 (2020).

44 Liao, M. *et al.* Single-cell landscape of bronchoalveolar immune cells in patients with COVID-19. *Nat Med* **26**, 842–844 (2020).

45 Akil, C., Xu, J., Shen, J. & Zhang, P. Unveiling the structural spectrum of SARS-CoV-2 fusion by in situ cryo-ET. *Nat Commun* **16**, 5150 (2025).

46 Miner, J. C. *et al.* Integrative structural studies of the SARS-CoV-2 spike protein during the fusion process (2022). *Curr Res Struct Biol* **4**, 220–230 (2022).

47 Cai, Y. *et al.* Distinct conformational states of SARS-CoV-2 spike protein. *Science* **369**, 1586–1592 (2020).

48 Xiong, X. *et al.* A thermostable, closed SARS-CoV-2 spike protein trimer. *Nat Struct Mol Biol* **27**, 934–941 (2020).

49 Zhang, J. *et al.* Structural impact on SARS-CoV-2 spike protein by D614G substitution. *Science* **372**, 525–530 (2021).

50 Muthuraman, K. *et al.* Human antibody targeting of coronavirus spike S2 subunit is associated with protection mediated by Fc effector functions. *J Virol* **99**, e0152325 (2025).

51 Wu, W. L. *et al.* Monoclonal antibody targeting the conserved region of the SARS-CoV-2 spike protein to overcome viral variants. *JCI Insight* **7** (2022).

52 Silwal, A. P. *et al.* DNA aptamers inhibit SARS-CoV-2 spike-protein binding to hACE2 by an RBD- independent or dependent approach. *Theranostics* **12**, 5522–5536 (2022).

53 Wang, S. *et al.* Identification of Covalent Cyclic Peptide Inhibitors Targeting Protein-Protein Interactions Using Phage Display. *J Am Chem Soc* **147**, 7461–7475 (2025).

54 Xue, S. *et al.* A novel cyclic gamma-AApeptide-based long-acting pan-coronavirus fusion

inhibitor with potential oral bioavailability by targeting two sites in spike protein. *Cell Discov* **8**, 88 (2022).

55 Thijssen, V. *et al.* A broad-spectrum macrocyclic peptide inhibitor of the SARS-CoV-2 spike protein. *Proc Natl Acad Sci U S A* **120**, e2303292120 (2023).

56 Wang, M. *et al.* Intranasal administration of broad-spectrum macrocyclic peptide inhibitor protects against SARS-CoV-2 Omicron variants. *Nat Commun* **17**, 1753 (2026).

57 Gaynor, K. U. *et al.* Multivalent bicyclic peptides are an effective antiviral modality that can potently inhibit SARS-CoV-2. *Nat Commun* **14**, 3583 (2023).

58 Moriyama, S. *et al.* Temporal maturation of neutralizing antibodies in COVID-19 convalescent individuals improves potency and breadth to circulating SARS-CoV-2 variants. *Immunity* **54**, 1841–1852 e1844 (2021).

59 Onodera, T. *et al.* A SARS-CoV-2 antibody broadly neutralizes SARS-related coronaviruses and variants by coordinated recognition of a virus-vulnerable site. *Immunity* **54**, 2385–2398 e2310 (2021).

60 Corman, V. M. *et al.* Detection of 2019 novel coronavirus (2019-nCoV) by real-time RT-PCR. *Euro Surveill* **25** (2020).

61 Mizutani, T., Fukushi, S., Saijo, M., Kurane, I. & Morikawa, S. Phosphorylation of p38 MAPK and its downstream targets in SARS coronavirus-infected cells. *Biochem Biophys Res Commun* **319**, 1228–1234 (2004).

62 Saso, W. *et al.* Significant role of host sialylated glycans in the infection and spread of severe acute respiratory syndrome coronavirus 2. *PLoS Pathog* **18**, e1010590 (2022).

63 Ohashi, H. *et al.* Potential anti-COVID-19 agents, cepharanthine and nelfinavir, and their usage for combination treatment. *iScience* **24**, 102367 (2021).

64 Fukushi, S. *et al.* Vesicular stomatitis virus pseudotyped with severe acute respiratory syndrome coronavirus spike protein. *J Gen Virol* **86**, 2269–2274 (2005).

65 Tani, H. *et al.* Involvement of ceramide in the propagation of Japanese encephalitis virus. *J Virol* **84**, 2798–2807 (2010).

66 Frilli, E., Amodeo, D., Cevenini, G., Nante, N. & Messina, G. Effectiveness of near-UVA in SARS-CoV-2 inactivation. *Epidemiol Infect* **151**, e76 (2023).

910 **Figure legends**

911 **Fig. 1. Identification of PA-001, a cyclic peptide showing potent anti-SARS-CoV-2 activity.**
912 (A) Schematic diagram of the flow to identify Spike-binding macrocyclic peptides and evaluate
913 their antiviral activity. The bottom arrows show the figures corresponding to the analyses shown
914 above. (B) Schematic representation of the mRNA display system to screen for Spike-binding
915 macrocyclic peptides. (C) Structure of PA-001. (D) PA-001 inhibited the propagation of SARS-
916 CoV-2. (a) Schematic representation of SARS-CoV-2 infection assay. VeroE6/TMPRSS2 cells
917 were inoculated with or without SARS-CoV-2 (Wk-521; wuhan strain) at an MOI of 0.003 for 1 h,
918 followed by washing out free virus and culturing cells with the medium supplemented with
919 indicated compounds for additional 24 h to detect viral proteins in cells by immunoblot (c) and to
920 quantify viral RNA in the culture supernatant by real time RT-PCR (d), as well as culturing cells
921 for 48 h to observe virus-induced cytopathic effect (CPE) by microscopic observation (b). In (c),
922 viral Spike (upper) and N (middle) proteins as well as cellular actin as an internal control (lower)
923 were detected. In (d), quantified viral RNAs were plotted against the concentration of treated
924 PA-001 (nM). (E) Pharmacokinetics of PA-001 in mice. (a) Scheme for treatment with PA-001
925 BALB/c mice and time points (1, 7, and 24 h post IP injection) of plasma collection. (b) BALB/c
926 mice were intraperitoneally administered with PA-001 at 10 mg/kg and were chased to obtain
927 plasma at 1, 7, and 24 h post-administration to quantify PA-001 concentration (mean ± SD).
928

929 **Fig. 2. PA-001 bound to FPPR in the S2 subunit and inhibited the membrane fusion.**
930 (A) Binding of PA-001 to recombinant SARS-CoV-2 Spike protein of the full length (S1+S2), S1,
931 or S2 regions. Each recombinant Spike protein was immobilized and incubated with HA-tagged
932 PA-001 at various concentrations up to 100 nM, followed by washing out and detection with
933 horseradish peroxidase (HRP)-conjugated anti-HA antibody. (B) Schematic model for the SARS-
934 CoV-2 entry process, in which viral attachment to cells via Spike-ACE2 binding is followed by the
935 fusion of viral envelope with cellular membrane either on the cell surface or in the
936 endosome/lysosome. (C) (a) Virus-cell attachment assay. VeroE6/TMPRSS2 cells were
937 exposed to SARS-CoV-2 at an MOI of 0.01 at 4°C for 15 min in the presence or absence of
938 casirivimab (CAS) + imdevimab (IMD) (50, 500, or 5,000 ng/mL), mefloquine (MFQ) (0.4, 2, or 10
939 μM), or PA-001 (40, 200, or 1,000 nM), and were then washed out to quantify cell-bound viral RNA
940 by real-time RT-PCR. Ordinary one-way ANOVA followed by Dunnett's multiple comparisons with
941 the DMSO control was performed (*: $p<0.05$, **: $p<0.01$, ***: $p<0.001$, ****: $p<0.0001$). (b) Cell-
942 cell fusion assay. Spike-overexpressing HEK293T cells carrying the LgBiT gene were co-
943 cultured with ACE2-expressing VeroE6/TMPRSS2 cells carrying the HiBiT gene upon treatment
944 with or without varying concentrations (up to 200 nM) of PA-001 for 1 h to detect luciferase activity
945 to evaluate fusion activity mediated by Spike and ACE2. IC_{50} of PA-001 is also indicated. (D)
946 Induction of PA-001-resistant SARS-CoV-2 variants. (a) Schematic representation of the
947 infection assay for inducing PA-001-resistant SARS-CoV-2 clones. SARS-CoV-2-infected

948 VeroE6/TMPRSS2 cells were continuously cultured with PA-001 at 1,000 nM for 24-48 h (Passage
949 0). The resultant culture supernatants were collected and diluted to 10-fold, which were then
950 inoculated to naive VeroE6/TMPRSS2 cells in the presence of 1,000 nM PA-001 and cultured for
951 24 h (Passage 1). The culture supernatants were repeatedly collected and then inoculated to
952 the cells upon 1,000 nM PA-001 for the next passage. At passage 7, the culture supernatants
953 were extracted from eight independent cultures (A8 – H8). (b) PA-001 sensitivity of the collected
954 supernatant clones. VeroE6/TMPRSS2 cells were inoculated with these collected supernatants
955 or the parental virus (WT) upon treatment with varying concentrations of PA-001 (left) or RDV as
956 a reference (right) to determine virus RNA levels in the culture supernatants as shown in Fig. 1D-
957 d. (E) Amino acid sequence of the PA-001-resistant clones. (a) Upper, schematic structure for
958 the SARS-CoV-2 Spike protein. Lower, amino acid sequence of the clones, A8–H8, as well as
959 the parental virus (WT). The substituted amino acids are highlighted by red. The amino acid
960 numbers are indicated. (b) Structure of Spike trimer in the pre-fusion (left, PDB: 6XR8),
961 intermediation (center, PDB: 8Z7P), and post-fusion (right, PDB: 8FDW) forms. Red color
962 indicates the mutated amino acids shown in (a). Blue color indicates FP. (F) Binding capacity
963 of recombinant SARS-CoV-2 Spike carrying the L841R and P862Q substitutions to PA-001. (a)
964 Each recombinant Spike (WT, L841R, and P862Q) was immobilized and incubated with HA-
965 tagged PA-001 (PA-001-HA) at varying concentrations in the presence (gray, competition) or
966 absence (red, S-PA001 binding) of non-tagged PA-001 at 10 μM. After washing out, bound HA-
967 PA-001 was visualized with HRP-conjugated anti-HA antibody. Samples without Spike-
968 immobilization were also prepared to define the background signal (green). (b) Binding signals
969 with Spike WT (left), Spike L841R (center), and Spike P862Q (right) are plotted against the
970 concentrations of treated PA-001-HA. Ordinary two-way ANOVA followed by
971 tukey's multiple comparisons was performed (*: $p<0.05$, **: $p<0.01$, ***: $p<0.001$). (G) Cell fusion
972 assay performed as described in Fig. 2C-b using the cells overexpressing either Spike WT, L841R,
973 or P862Q co-cultured with ACE2-expressing cells upon PA-001 treatment at various
974 concentrations.
975
976 **Fig. 3. PA-001 showed a broad anti-SARS-CoV-2 activity against multiple variants.**
977 (A) Antiviral activity of PA-001 and casirivimab + imdevimab against the SARS-CoV-2 variants
978 (Wuhan, Alpha, Beta, Gamma, Delta, and Omicrons BA.1.18 and XBB.1.16). Drug response
979 was evaluated as described in Fig. 1D-d, using each SARS-CoV-2 variant as inoculum. (B)
980 Sequence homology from aa 834 to 863 in Spike among the SARS-CoV2 variants. Asterisks
981 indicate the fully homologous sites among all the variants.
982
983 **Fig. 4. PA-001 inhibited viral propagation and disease progression in mice and hamsters.**
984 (A) (a) Scheme for prophylactic treatment with PA-001 to SARS-CoV-2-infected hamsters.
985 Golden Syrian hamsters (n = 7 for infected groups and n = 5 for uninfected group) were

986 intraperitoneally treated with PA-001 (0.3, 1.0, or 3.0 mg/kg) or the vehicle at day -0.5, -0.08,
987 0.5,1.0, and 1.5 (-12, -2, 12, 24, and 36 h) post-inoculation, and were inoculated with SARS-CoV-
988 2 (3.48×10^3 $TCID_{50}$/hamster) intranasally at day 0. Lungs were collected at day 2 post-
989 inoculation. (b) Infectious viral titer in the lungs at day 2 was quantified. Black, vehicle; light
990 red, 0.3 mg/kg PA-001; red, 1.0 mg/kg PA-001; dark red, 3.0 mg/kg PA-001. Ordinary one-way
991 ANOVA followed by Dunnett's multiple comparisons with the vehicle control was performed (*:
992 $p<0.05$, **: $p<0.01$, ***: $p<0.001$). (B) (a) Scheme for therapeutic treatment with PA-001 to
993 SARS-CoV-2-infected mice. BALB/c mice (n = 8) were intranasally inoculated with mouse-
994 adopted SARS-CoV-2 (QHmusX) (3×10^3 $TCID_{50}$/mouse) (day 0) and then administered
995 intraperitoneally with PA-001 (10 or 30 mg/kg), CAS + IMD (10 mg/kg), or the vehicle control at
996 day 0.04, 0.3, 1, 2, 3, and 4 (1, 8, 24, 48, 72, and 96 h). The mice were chased to examine the
997 body weight as well as survival ratio. (b, c) Survival rate (b) and body weight (body weight at
998 day 0 as 100%) (c) along with the time course after virus inoculation (day) was plotted. Black,
999 vehicle; gray, 10 mg/kg CAS + IMD; red, 10 mg/kg PA-001; dark red, 30 mg/kg PA-001. Ordinary
1000 two-way ANOVA followed by Dunnett's multiple comparisons with the PBS control was performed
1001 (*: $p<0.05$, **: $p<0.01$, ***: $p<0.001$, ****: $p<0.0001$). (C) (a) Schematic diagram for PA-001
1002 treatment after SARS-CoV-2 infection to hamsters. Golden Syrian hamsters (n = 6) intranasally
1003 inoculated with SARS-CoV-2 (2.11×10^5 $TCID_{50}$/hamster) (day 0) were intraperitoneally treated
1004 with PA-001 (1.0 or 5.0 mg/kg) or the vehicle at day 0.08, 0.3, 1.0, 2.0, and 3.0 (2, 8, 24, 48, and
1005 72 h). Lungs were collected at day 5. (b) Body weight was observed daily, defining those at
1006 day 0 as 100%. Black, vehicle; red, PA-001 1.0 mg/kg; dark red, PA-001 5.0 mg/kg. Ordinary
1007 two-way ANOVA followed by Dunnett's multiple comparisons with the vehicle control was
1008 performed (*: $p<0.05$, **: $p<0.01$, ***: $p<0.001$, ****: $p<0.0001$). (c) SARS-CoV-2 RNA levels in
1009 the lung were quantified at day 5. Ordinary one-way ANOVA followed by Dunnett's
1010 multiple comparisons with the vehicle control was performed (*: $p<0.05$, **: $p<0.01$, ***: $p<0.001$).
1011 (d) Histopathology of the lungs at day 5. Lungs from hamsters of each treatment group were
1012 stained by HE.
1013
1014 **Fig. 5. Augmented anti-SARS-CoV-2 profiles by combination treatment with PA-001 and**
1015 **RDV**.
1016 (A) Combination treatment with PA-001 and RDV in cell-based infection assay. Antiviral activities
1017 were evaluated as described in Fig. 1D-d, using SARS-CoV-2-infected VeroE6/TMPRSS2 cells
1018 that were treated with combinations of various concentrations of PA-001 (0, 0.04, 0.18, 0.70, 2.8,
1019 and 11.2 nM) and RDV (0, 750, 1,500, 3,000, 6,000, and 12,000 nM). (B) (a) Scheme for post-
1020 administration of combination with PA-001 and the RDV metabolite, GS-441524 (RDV-m).
1021 BALB/c mice were intranasally inoculated with SARS-CoV-2 (2.3×10^3 $TCID_{50}$/mouse) and then
1022 intraperitonially administered with either GS-441524 (25 mg/kg (day 1) and 12.5 mg/kg (days 2,
1023 3)) alone, GS-441524 (25 mg/kg (day 1) and 12.5 mg/kg (days 2, 3)) with PA-001 (26 mg/kg), or

1024 the vehicle once daily from day 1 to 3. Mice were euthanized at day 3 without dosing on the day
1025 for collecting lungs and sera (n = 4) and day 10 after monitoring survival rate and body weight (n
1026 = 5-7). (b, c) Survival rate (b) and body weight (c) until day 10 for each group are shown. Black,
1027 vehicle; blue, GS-441524; red, GS-441524 + PA-001. Ordinary two-way ANOVA followed by
1028 tukey's multiple comparisons was performed (*: $p<0.05$, **: $p<0.01$, ***: $p<0.001$, ****: $p<0.0001$).
1029 (d, e) Infectious viral titer in the lung (d) and the lung weight (e, lung weight-to-body weight ratio)
1030 at day 3 are shown. Ordinary one-way ANOVA followed by tukey's multiple comparisons was
1031 performed (*: $p<0.05$, **: $p<0.01$, ***: $p<0.001$). (C) Production of the cytokines related with the
1032 disease severity, IL-6, TNF-α, IL-1β, GCSF, IFN-γ, IP-10, MIP-1α, and MCP-1, from the serum
1033 and the lung at day 3 were analyzed. Ordinary one-way ANOVA followed by
1034 tukey's multiple comparisons was performed (*: $p<0.05$, **: $p<0.01$, ***: $p<0.001$).
1035
1036 **Fig. 6. Safety and pharmacokinetics profiles of PA-001 single administration to healthy**
1037 **volunteers.**
1038 (A) Baseline characteristics of 32 participants in the phase I trial for PA-001. The indicated
1039 profiles are presented as mean ± standard deviation for each cohort group (Placebo, 18 mg PA-
1040 001, 64 mg PA-001, 128 mg PA-001, and 128 mg PA-001 to elderly adults). Numbers of
1041 participants for each group are also shown (n = 6 or 8 for each group). (B) Number of
1042 participants as well as percentage showing the treatment-related treatment emergent adverse
1043 effects (TEAEs) as indicated for each cohort group. (C) Plasma concentrations of PA-001 for
1044 each cohort (closed circle, 18 mg; closed diamond, 64 mg; closed square, 128 mg; open
1045 square,128 mg to elderly adults) in the single-dose sequential-group study (Part A) are plotted
1046 against the time post intravenous infusions in healthy subjects. (D) Pharmacokinetic parameters
1047 calculated based on the profile shown in (C). $AUC_{0\text{-tlast}}$, area under the concentration-time curve
1048 from time 0 to the endpoint; $AUC_{0\text{-}24}$, area under the concentration-time curve from 0 to 24 h; C_{max},
1049 maximum concentration; T_{max}, time for maximum concentration; $T_{1/2}$, half-life. Data are
1050 represented as mean ± standard deviation.
1051

Fig. 1

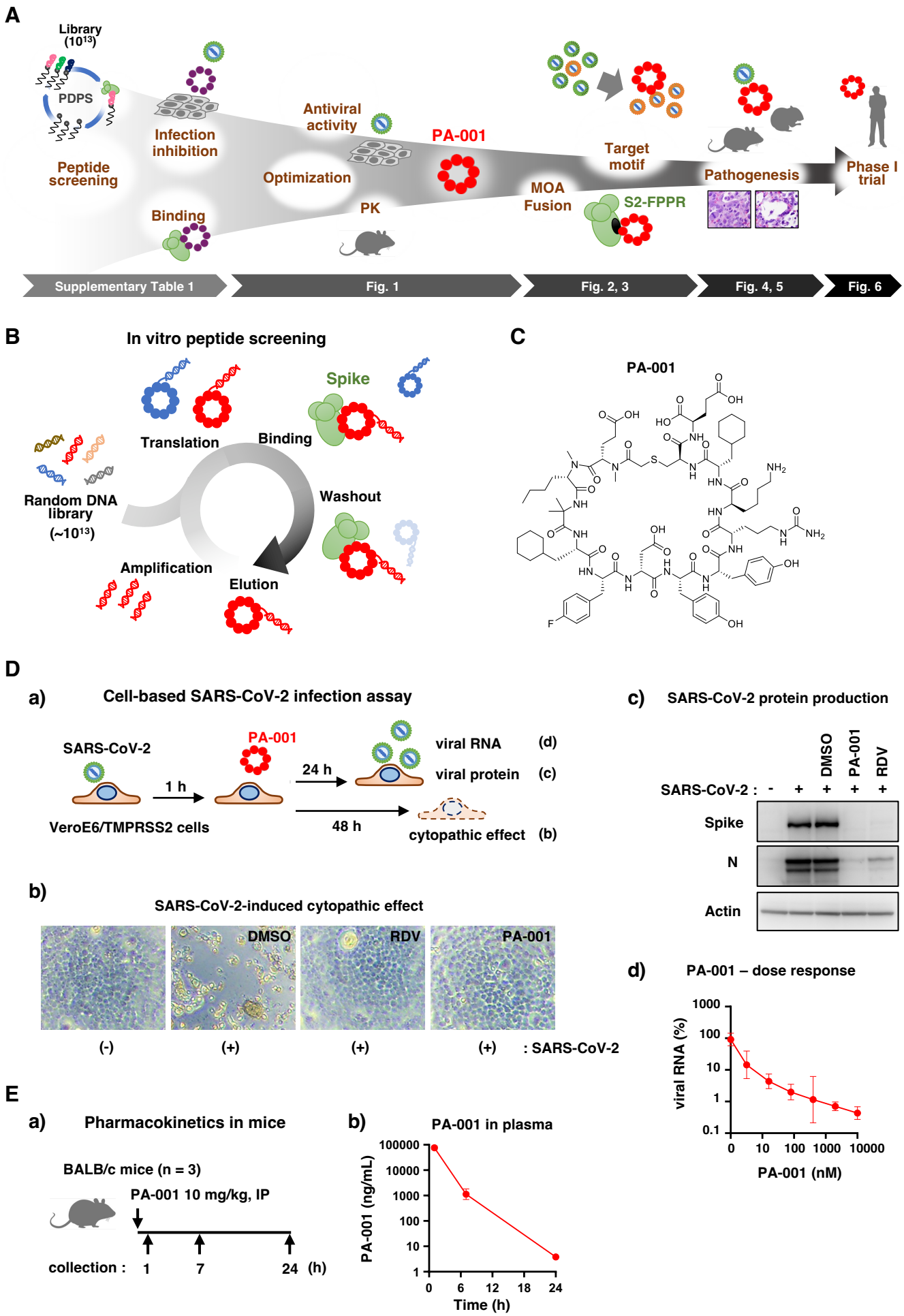
A
Library (10^13)
PDPS
Peptide screening
Infection inhibition
Binding
Antiviral activity
Optimization
PK
PA-001
Target motif
MOA Fusion
S2-FPPR
Pathogenesis
Phase I trial
Supplementary Table 1
Fig. 1
Fig. 2, 3
Fig. 4, 5
Fig. 6
B
In vitro peptide screening
Random DNA library (~10^13)
Translation
Binding
Spike
Washout
Elution
Amplification
C
PA-001
D
a)
Cell-based SARS-CoV-2 infection assay
SARS-CoV-2
PA-001
1 h
24 h
48 h
VeroE6/TMPRSS2 cells
viral RNA (d)
viral protein (c)
cytopathic effect (b)
b)
SARS-CoV-2-induced cytopathic effect
DMSO
RDV
PA-001
(-)
(+)
(+)
(+)
: SARS-CoV-2
c)
SARS-CoV-2 protein production
DMSO
PA-001
RDV
SARS-CoV-2 : - + + + +
Spike
N
Actin
d)
PA-001 – dose response
viral RNA (%)
1000
100
10
1
0.1
0
10
100
1000
10000
PA-001 (nM)
E
a)
Pharmacokinetics in mice
BALB/c mice (n = 3)
PA-001 10 mg/kg, IP
collection : 1 7 24 (h)
b)
PA-001 in plasma
PA-001 (ng/mL)
100000
10000
1000
100
10
1
0
6
12
18
24
Time (h)

Fig. 2

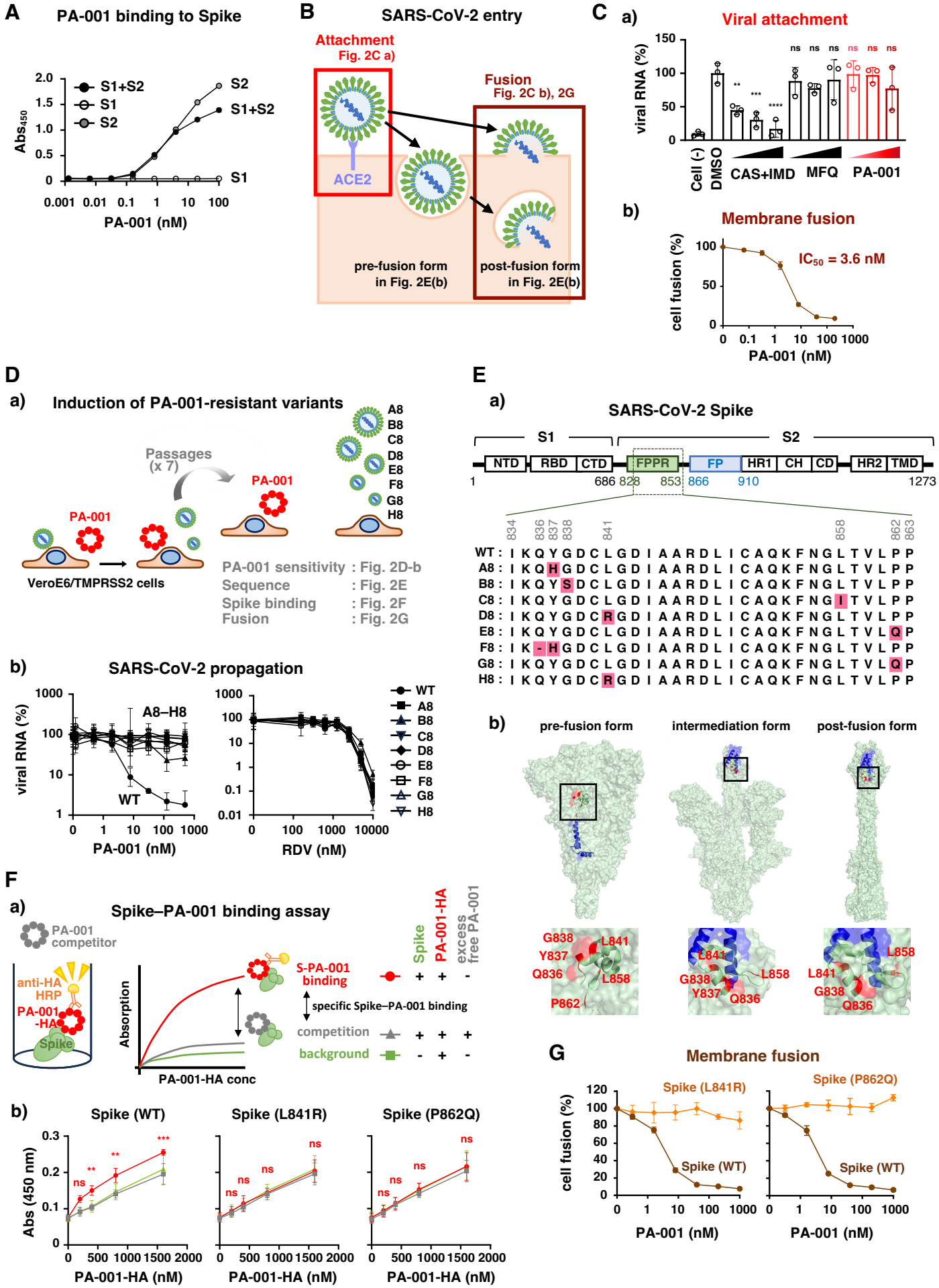
A
PA-001 binding to Spike
S1+S2
S1
S2
S2
S1+S2
S1
Abs450
PA-001 (nM)
B
SARS-CoV-2 entry
Attachment
Fig. 2C a)
Fusion
Fig. 2C b), 2G
ACE2
pre-fusion form
in Fig. 2E(b)
post-fusion form
in Fig. 2E(b)
C
a)
Viral attachment
viral RNA (%)
Cell (-)
DMSO
CAS+IMD
MFQ
PA-001
b)
Membrane fusion
cell fusion (%)
IC50 = 3.6 nM
PA-001 (nM)
D
a)
Induction of PA-001-resistant variants
Passages
(x 7)
PA-001
PA-001
VeroE6/TMPRSS2 cells
A8
B8
C8
D8
E8
F8
G8
H8
PA-001 sensitivity : Fig. 2D-b
Sequence : Fig. 2E
Spike binding : Fig. 2F
Fusion : Fig. 2G
b)
SARS-CoV-2 propagation
viral RNA (%)
A8–H8
WT
PA-001 (nM)
RDV (nM)
WT
A8
B8
C8
D8
E8
F8
G8
H8
E
a)
SARS-CoV-2 Spike
S1
S2
NTD
RBD
CTD
FPPR
FP
HR1
CH
CD
HR2
TMD
1
686 828
853
866
910
1273
WT : I K Q Y G D C L G D I A A R D L I C A Q K F N G L T V L P P
A8 : I K Q H G D C L G D I A A R D L I C A Q K F N G L T V L P P
B8 : I K Q Y S D C L G D I A A R D L I C A Q K F N G L T V L P P
C8 : I K Q Y G D C L G D I A A R D L I C A Q K F N G I T V L P P
D8 : I K Q Y G D C R G D I A A R D L I C A Q K F N G L T V L P P
E8 : I K Q Y G D C L G D I A A R D L I C A Q K F N G L T V L Q P
F8 : I K - H G D C L G D I A A R D L I C A Q K F N G L T V L P P
G8 : I K Q Y G D C L G D I A A R D L I C A Q K F N G L T V L Q P
H8 : I K Q Y G D C R G D I A A R D L I C A Q K F N G L T V L P P
b)
pre-fusion form
intermediation form
post-fusion form
G838
L841
Y837
Q836
L858
P862
L841
G838
Y837
Q836
L858
L858
L841
G838
Q836
F
a)
Spike–PA-001 binding assay
PA-001
competitor
anti-HA
HRP
PA-001
-HA
Spike
Absorption
PA-001-HA conc
S-PA-001
binding
Spike
PA-001-HA
excess
free PA-001
specific Spike–PA-001 binding
competition
background
b)
Spike (WT)
Spike (L841R)
Spike (P862Q)
Abs (450 nm)
PA-001-HA (nM)
PA-001-HA (nM)
PA-001-HA (nM)
G
Membrane fusion
Spike (L841R)
Spike (P862Q)
Spike (WT)
Spike (WT)
cell fusion (%)
PA-001 (nM)
PA-001 (nM)

Fig. 3

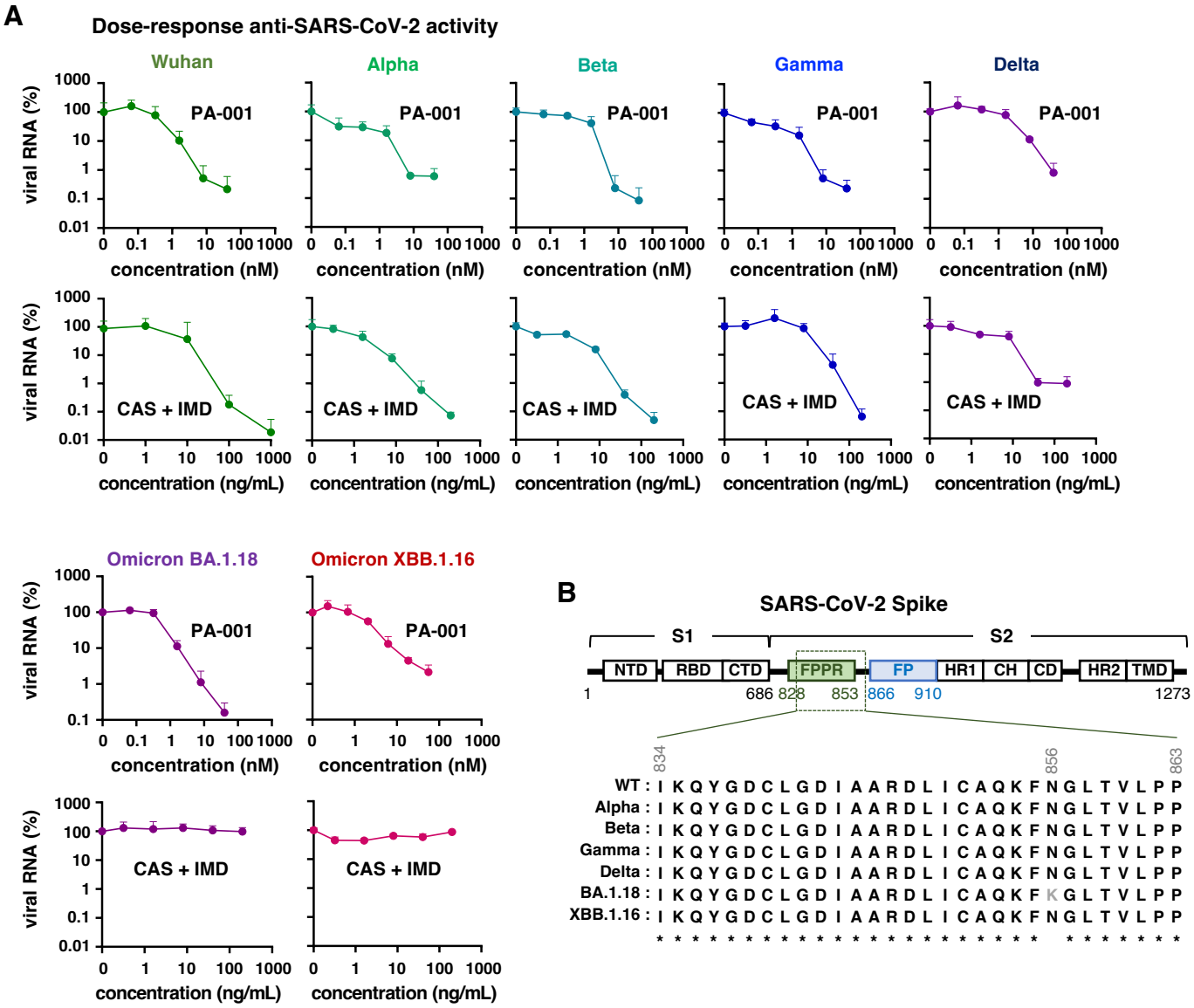
A
Dose-response anti-SARS-CoV-2 activity
Wuhan
Alpha
Beta
Gamma
Delta
Omicron BA.1.18
Omicron XBB.1.16
PA-001
CAS + IMD
viral RNA (%)
concentration (nM)
concentration (ng/mL)
B
SARS-CoV-2 Spike
S1
S2
NTD
RBD
CTD
FPPR
FP
HR1
CH
CD
HR2
TMD
1
686
828
853
866
910
1273
834
856
863
WT : I K Q Y G D C L G D I A A R D L I C A Q K F N G L T V L P P
Alpha : I K Q Y G D C L G D I A A R D L I C A Q K F N G L T V L P P
Beta : I K Q Y G D C L G D I A A R D L I C A Q K F N G L T V L P P
Gamma : I K Q Y G D C L G D I A A R D L I C A Q K F N G L T V L P P
Delta : I K Q Y G D C L G D I A A R D L I C A Q K F N G L T V L P P
BA.1.18 : I K Q Y G D C L G D I A A R D L I C A Q K F K G L T V L P P
XBB.1.16 : I K Q Y G D C L G D I A A R D L I C A Q K F N G L T V L P P

Fig. 4

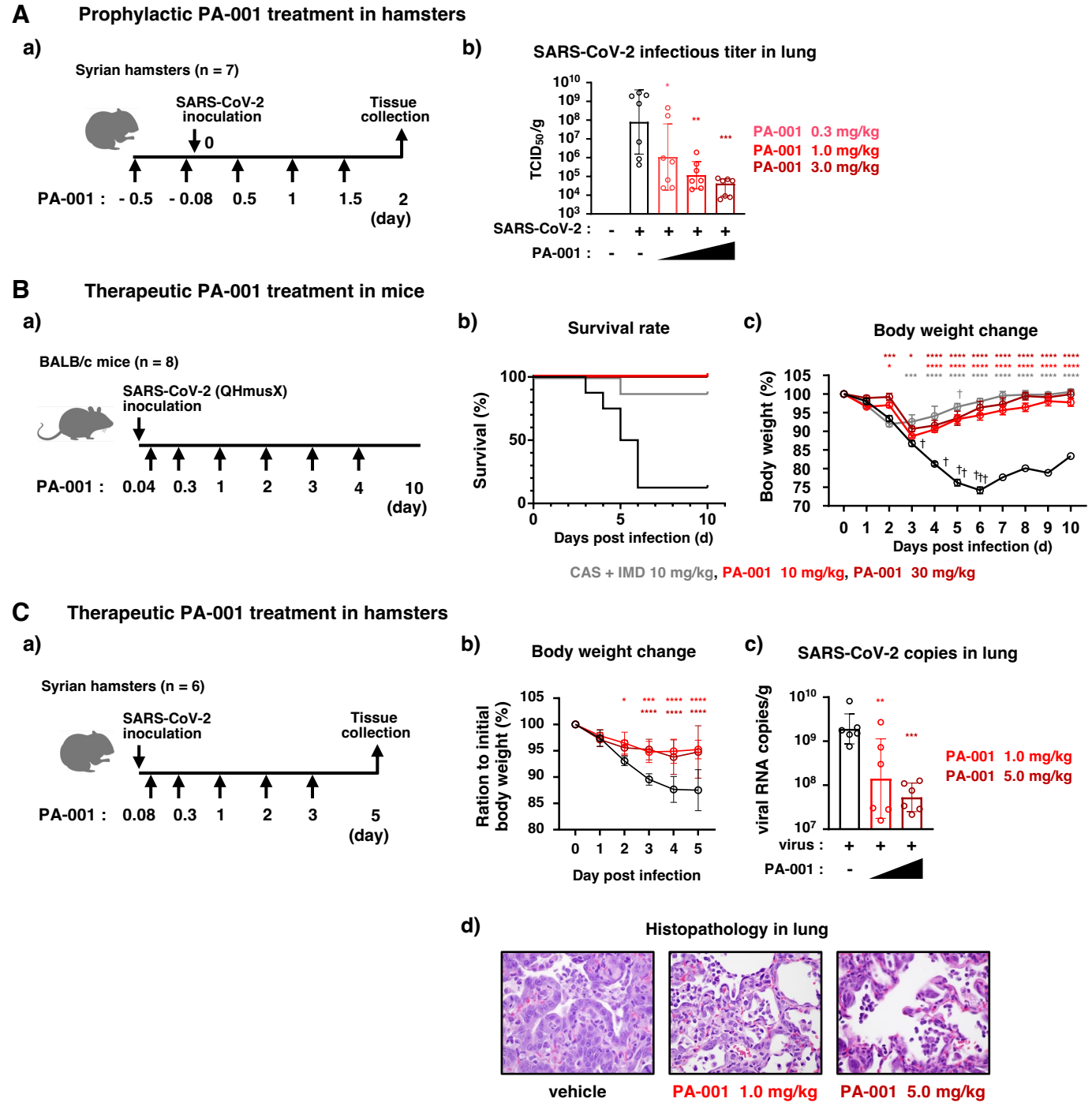
A
Prophylactic PA-001 treatment in hamsters
a)
Syrian hamsters (n = 7)
SARS-CoV-2 inoculation
Tissue collection
0
PA-001 : - 0.5 - 0.08 0.5 1 1.5 2 (day)
b)
SARS-CoV-2 infectious titer in lung
TCID50/g
PA-001 0.3 mg/kg
PA-001 1.0 mg/kg
PA-001 3.0 mg/kg
SARS-CoV-2 : - + + + +
PA-001 : - -
B
Therapeutic PA-001 treatment in mice
a)
BALB/c mice (n = 8)
SARS-CoV-2 (QHmusX) inoculation
PA-001 : 0.04 0.3 1 2 3 4 10 (day)
b)
Survival rate
Survival (%)
Days post infection (d)
c)
Body weight change
Body weight (%)
Days post infection (d)
CAS + IMD 10 mg/kg, PA-001 10 mg/kg, PA-001 30 mg/kg
C
Therapeutic PA-001 treatment in hamsters
a)
Syrian hamsters (n = 6)
SARS-CoV-2 inoculation
Tissue collection
PA-001 : 0.08 0.3 1 2 3 5 (day)
b)
Body weight change
Ration to initial body weight (%)
Day post infection
c)
SARS-CoV-2 copies in lung
viral RNA copies/g
PA-001 1.0 mg/kg
PA-001 5.0 mg/kg
virus : + + +
PA-001 : -
d)
Histopathology in lung
vehicle
PA-001 1.0 mg/kg
PA-001 5.0 mg/kg

Fig. 5

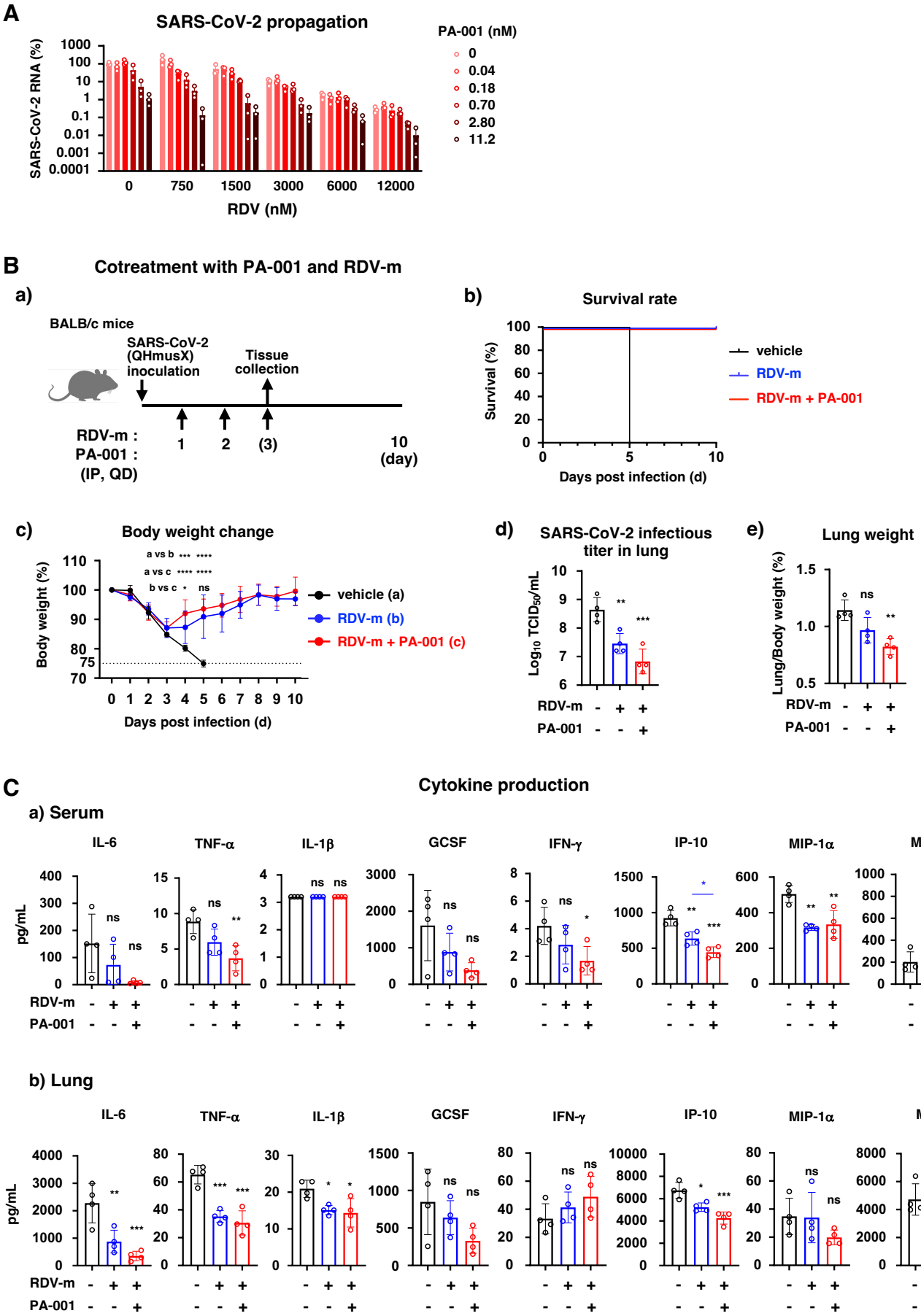
A
SARS-CoV-2 propagation
SARS-CoV-2 RNA (%)
1000
100
10
1
0.1
0.01
0.001
0.0001
0
750
1500
3000
6000
12000
RDV (nM)
PA-001 (nM)
0
0.04
0.18
0.70
2.80
11.2
B
Cotreatment with PA-001 and RDV-m
a)
BALB/c mice
SARS-CoV-2 (QHmusX) inoculation
Tissue collection
RDV-m :
PA-001 :
(IP, QD)
1
2
(3)
10 (day)
b)
Survival rate
Survival (%)
Days post infection (d)
vehicle
RDV-m
RDV-m + PA-001
c)
Body weight change
Body weight (%)
a vs b *** ****
a vs c **** ****
b vs c * ns
vehicle (a)
RDV-m (b)
RDV-m + PA-001 (c)
Days post infection (d)
d)
SARS-CoV-2 infectious titer in lung
Log10 TCID50/mL
RDV-m
PA-001
e)
Lung weight
Lung/Body weight (%)
ns
RDV-m
PA-001
C
Cytokine production
a) Serum
IL-6
TNF-α
IL-1β
GCSF
IFN-γ
IP-10
MIP-1α
MCP-1
pg/mL
RDV-m
PA-001
b) Lung
IL-6
TNF-α
IL-1β
GCSF
IFN-γ
IP-10
MIP-1α
MCP-1
pg/mL
RDV-m
PA-001

Fig. 6

A

Subject demographics and baseline characteristics

Demographic	Placebo (N = 8)	18 mg PA-001 (N = 6)	64 mg PA-001 (N = 6)	128 mg PA-001 (N = 6)	128 mg PA-001 (Elderly) (N = 6)	Overall (N = 32)
Age [years; range]	46.6 ± 14.20 [32-66]	38.7 ± 9.05 [30-55]	41.7 ± 14.18 [22-57]	37.2 ± 15.72 [23-59]	69.8 ± 3.71 [66-75]	46.8 ± 16.49 [22-75]
Sex						
Female	4 (50.0%)	2 (33.3%)	3 (50.0%)	5 (83.3%)	5 (83.3%)	19 (59.4%)
Male	4 (50.0%)	4 (66.7%)	3 (50.0%)	1 (16.7%)	1 (16.7%)	13 (40.6%)
Race						
White	7 (87.5%)	3 (50.0%)	2 (33.3%)	3 (50.0%)	6 (100%)	21 (65.6%)
Black or African American	1 (12.5%)	2 (33.3%)	4 (66.7%)	3 (50.0%)	---	10 (31.3%)
Multiple	---	1 (16.7%)	---	---	---	1 (3.1%)
Ethnicity						
Not Hispanic or Latino	5 (62.5%)	3 (50.0%)	5 (83.3%)	3 (50.0%)	4 (66.7%)	20 (62.5%)
Hispanic or Latino	3 (37.5%)	3 (50.0%)	1 (16.7%)	3 (50.0%)	2 (33.3%)	12 (37.5%)
Height (cm)	166.86 ± 8.522	172.03 ± 7.989	174.17 ± 10.809	169.28 ± 12.378	163.53 ± 6.087	169.03 ± 9.495
Body weight (kg)	74.640 ± 12.6180	74.700 ± 9.4240	84.650 ± 8.3050	76.770 ± 21.1180	65.130 ± 11.0530	75.140 ± 13.8040
Body Mass Index (kg/m^2)	26.75 ± 3.492	25.15 ± 1.231	27.97 ± 2.373	26.42 ± 4.118	24.38 ± 4.090	26.17 ± 3.299

B

Adverse effect of PA-001

Treatment-related TEAEs	Placebo (N = 8)	18 mg PA-001 (N = 6)	64 mg PA-001 (N = 6)	128 mg PA-001 (N = 6)	128 mg PA-001 (Elderly) (N = 6)
Overall	1 (12.5%)	-	2 (33.3%)	-	-
mild	1 (12.5%)	-	2 (33.3%)	-	-
Serious	-	-	-	-	-
Discontinuation	-	-	-	-	-
Death	-	-	-	-	-

C

PA-001 in plasma

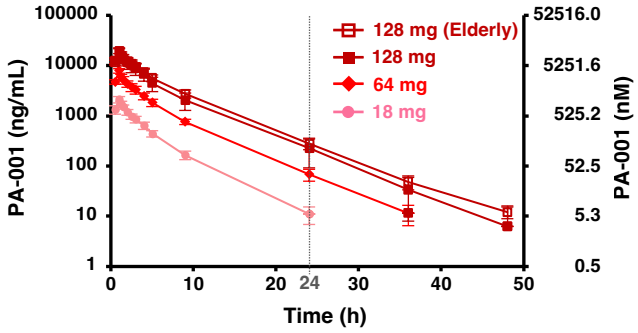

D

Pharmacokinetic parameters of PA-001 in healthy volunteers

Parameter	18 mg PA-001	64 mg PA-001	128 mg PA-001	128 mg PA-001 (Elderly)
$AUC_{0\text{-}tlast}$ (h*ng/mL)	7,050.0±910.0	28,200.0±3,190.0	74,200.0±21,900.0	85,100.0±12,500.0
$AUC_{0\text{-}24}$ (h*ng/mL)	7,050.0±910.0	27,900.0±3,260.0	72,800.0±21,100.0	83,200.0±12,100.0
C_{max} (ng/mL)	2,130±279	7,860±814	18,300±4,240	19,000±2,220
T_{max} (h)	1.04±0.04	1.02±0.01	1.06±0.02	1.05±0.07
$T_{1/2}$ (h)	3.61±0.63	4.41±0.51	4.46±0.54	4.79±0.35